AL ZAHRAA UNIVERSITY JOURNAL
Health and Medical Science

*Al-Zahraa Journal for Health and Medical Sciences 2026; 4(1):*25-50 **Vol. 4, No.1, 2026**
www.zjhms.alzahraa.edu.iq

Novel Nano Schiff Base Ligand and Its Metal Complexes: Synthesis, Characterization, Molecular Docking, Antibacterial, Anticancer Evaluation Against PC-3 Cells

Nesser Kadham Shareef [1,2*], Fawzi Yahya Wadday[2]

[1]Department of Chemistry , Faculty of Science ,Kerbala University ,Karbala –Iraq
[2]Department of Chemistry, Faculty of Science, Kufa University, Al-Najaf-Iraq

* fawzi.almwuashi@uokufa.edu.iq naseer.k@uokerbala.edu.iq

Received: 05 February (2026), Accepted: 19 March 2026. Published: 31 March 2026

ABSTRACT

(1Z,2Z)-1,2-diphenyl-N1,N2-bis(pyridin-2-ylmethyl)ethane-1,2-diimine methanimine (DBED) L_1, a new nanoligand, was produced by the condensation reaction of 1mole of 1,2-diphenylethane-1,2-dione with 2 mole of pyridin-2-ylmethanamine in anhydrous ethanol. Nano mononuclear complexes with Cu(II), Ag(I), and Au(III) ions generated by this ligand. The compounds were recognized by means of mass spectrometry, ^{1}HNMR spectroscopy, elemental analysis (C,H,N,O),atomic absorption, (UV-Vis) spectroscopy, (FT-IR) spectroscopy ,magnetic susceptibility, molar conductivity, while the XRD, and FE-SEM revealed purity for the compounds and their crystal structure flaws when ligands become metal complexes. The elemental analysis and metal complexes composition data showed that the metal-to-ligand ratio is [M(L)], where M is Cu(II), Ag(I), and Au(III), and (DBED)L_1 is an azomethine ligand. Proposed structure is tetrahedral for Ag(I) complex, square planar for Au(III) complex whereas the Cu(II) compound has an octahedral geometry were discussed. Copper complex were non-conductive, but all others were electrolytic. The compounds were temporally stable and inhibited pathogenic *Staphylococcus. aureus* and *Escherichia. coli*. The study also examined the toxicity of (DBED)$L_1$and its Au(III) complex to human prostate cancer cells (PC-3) and other normal cells in vitro .Au(III) complex has a stronger affinity for cancer cells than the ligand but no effect on non-cancer cells. DFT estimated molecular energy levels with B3LYP/631G basis set. Au(III) complex and (DBED)L_1 were optimally placed at receptor crucial regions using Molecular Operating Environment (MOE). These results suggest that the Au(III) complex exhibits promising in vitro anticancer activity against prostate cancer cells.

Keywords: Prostate cancer, Molecular docking, Antibacterial activity, ^{1}HNMR spectroscopy

Al-Zahraa Journal for Health and Medical Sciences 2026; 4(1):25-50 **Vol. 4, No.1, 2026**
www.zjhms.alzahraa.edu.iq

1. Introduction

Schiff bases, exhibiting a pronounced chelating affinity for various transition metal ions, have garnered significant interest in coordination chemistry. Specifically, Schiff base chelates with multiple donor atoms are robust π-ligands that consequently yield stable complexes[1] . Such complexes exhibited intriguing properties that varied between chemical and physical. They possess a wide range of pharmacological activities. Chelation increase antibacterial and anticancer activity, according to growing research. This feature may be ascribed to the interaction between electron-deficient transition metal ions and electron-rich DNA or proteins[2]. Thus Schiff base and their metals complexes plays a significant role in triggering the generation of reactive oxygen species (ROS) and subsequently inducing cellular stress and leading to the demise of cancer cells[3] . The second biggest cause of death for males is prostate cancer (PC-3). Early clinical diagnosis techniques can play a significant role in curing PC-3 and significantly extending the life span of patients. In order to diagnose early stage prostate cancer, The prostate-specific antigen (PSA) blood test is commonly utilized as a screening tool [4]. Multiple variables may elevate the likelihood of acquiring prostate cancer. These include, advanced age (it is more common after the age of 50).Race (Black men are at a higher risk).Family history of the disease and obesity[5]. A recent report showed that the peripheral zone of the prostate held approximately 3000nM Zn^{2+} per gram, while the cancerous prostate held only 600nM per gram [6]. It is commonly believed that utilizing Zn^{2+} depletion as a biomarker for early detection of PC-3 requires the combination of a decrease in Zn^{2+} and the decrease in citrate. In the same way as Zn^{2+}, the amount of citrate decreased in PC-3 from 13,000 nM/g of normal cells to 1000 nM/g of tumor prostate cells [6]. The most important thing to note is that some of Schiff base metal complexes were found to be less harmful to normal human liver cells (HL-7702) compared to cisplatin. But The strength of these compounds as chemotherapeutic agents is largely dependent on the kind of metal and the intricacy of the Schiff base. For example as recent , copper complexes are employed as potent anticancer drugs[7]. Abdou S. et al. Analyze Cu complexes NPs anticancer efficacy on cell lines that represent prostate cancer. This characteristic is linked to the attachment of Cu complex nanoparticles (NPs) to DNA strands, which inhibits DNA replication and mitosis prostate cancer cell lines [8].

AL ZAHRAA UNIVERSITY JOURNAL
Health and Medical Science

*Al-Zahraa Journal for Health and Medical Sciences 2026; 4(1):*14-50 **Vol. 4, No.1, 2026**
www.zjhms.alzahraa.edu.iq

Here Nano metal complexes are synthesized from Schiff bases, which result from the condensation of 1,2-Diphenylethane-1,2-dione and pyridin-2-ylmethanamine. An analysis was performed on the newly synthesized complexes of copper (II), silver(I) and gold (III), also the antibacterial activity was evaluated against Staphylococcus aureus and Escherichia coli strains utilizing the paper disc diffusion method (for qualitative assessment) and the serial dilutions in liquid broth technique (for determining the minimum inhibitory concentration). The gold (III) complex and L_1 were evaluated for their antiproliferative effects on PC-3 prostate cancer cell lines. The mechanism of action of these drugs was elucidated through molecular docking studies, which demonstrate the effective binding of molecules to the proteins active site. In addition, the synthesized compounds were screened for in vitro .The half-maximal inhibitory concentration (IC_{50}) values confirmed selective toxicity. The IC_{50} values for PC-3 cancer cells were 71.49 µg/mL for L_1 and 51.48µg/mL for gold(III) complex. Normal HDF cells had IC_{50} values of 2693.32 µg/mL and 817.24 µg/mL, respectively. These results suggest that the gold(III) complex selectively harms prostate cancer cells over normal cells, supporting its potential as a novel anticancer therapy.

2. Experimental

2.1 Materials

pyridin-2-ylmethanamine, 1,2-Diphenylethane-1,2-dione, metal chlorides $CuCl_2.2H_2O$, $H[AuCl_4]$and $AgNO_3$, as well as Müller-Hinton agar, absolute ethanol, glacial acetic acid, acetone, acetonitrile, diethyl ether, dimethylsulfoxide (DMSO), hexane, N,N-Dimethylformamide (DMF), ethyl acetate. All chemicals and solvents were of the highest quality and were sourced from Sigma-Aldrich. BDH and Fluka were employed without additional manipulation.

2.2 Instrumentation

Bruker D.R.X. (DMSO-d^6, 500 MHz) Stuart supplied the 1H nuclear magnetic resonance spectrometer, the 5975 quadrupole mass spectrometer, the Euro Vectro-3000A trace element analyzer, the Jena atomic absorption spectrometer (VARIO 6, AG), Shimadzu UV-visible spectrophotometer 1700 (wave length range 200-1100 nm), and Shimadzu Fourier transform

AL ZAHRAA UNIVERSITY JOURNAL
Health and Medical Science

*Al-Zahraa Journal for Health and Medical Sciences 2026; 4(1):*14-50 **Vol. 4, No.1, 2026**
www.zjhms.alzahraa.edu.iq

infrared spectrometer (wave length range 400-4000 cm^{-1}). Images of the compounds and their corresponding metals were obtained by scanning electron microscopy (FE-SEM) utilizing a Zeiss EM3200 microscope. X-ray diffraction (XRD) was conducted utilizing a Philips diffractometer, featuring a graphite crucible as the sole component. The apparatus utilized Cu Kα radiation (wave length = 1.54 Å) as the X-ray source at 45 kV and 50 mA. The concentration of chloride in Cu(II) and Au(III) complexes was quantified using $AgNO_3$ solutions. Thin layer chromatography (TLC) was utilized to ascertain the complete composition of the compounds. A selection of samples underwent activity evaluations at the Al-Ameen Center for Advanced Research and Biotechnology. Refrigerated centrifuge and the Marubeni freezer (-80 degrees Celsius) . Distillation apparatus the drying and sterilizing machinery .Incubators and readers. Inverted microscope . Microplates, multiwell plates, and 96-well plates . Microporous membranes capable of traversing a filter with a porosity of 0.22 μm. Sterilized containers for tissue culture (25.75 cm^2). Hydrothermal apparatus and water pump.

2.3 Synthesis of New ligand (L_1):

The synthesis of the ligand (1Z,2Z)-1,2-diphenyl-N1,N2-bis(pyridin-2-ylmethyl)ethane -1,2-diimine (L_1), (1.83 g ,0.017 mol) of pyridin-2-ylmethanamine was combined with (1.78 g ,0.0085 mol) of 1,2-Diphenylethane-1,2-dione, dissolved in 20 mL of hot 100% ethanol, to synthesize the (L_1) molecule, which was subsequently acidified with three drops of glacial acetic acid[9]. The reaction mixture was refluxed at 75°C with vigorous magnetic stirring to achieve homogeneity and regulate the nucleation process; this temperature was sustained for approximately 240 minutes to facilitate controlled thermal uniformity[9]. Upon completion of the reaction, heating was ceased, and the mixture was permitted to drop spontaneously to ambient temperature. The suspension was allowed to remain undisturbed for 8 hours to facilitate controlled crystallization and inhibit agglomeration. The reaction's progress was monitored via TLC with hexane–ethanol (4:6) (v/v) as the eluent, resulting in the creation of a yellow crystalline compound. Subsequently, cold dry ether was employed to filter and cleanse the chemical [10]. Subsequent to oven drying, the yield of the solid was 87%. Scheme (1) depicts the reaction for the formation of (L_1).

IRAQI Academic Scientific Journals

AL ZAHRAA UNIVERSITY JOURNAL
Health and Medical Science

*Al-Zahraa Journal for Health and Medical Sciences 2026; 4(1):*14-50 **Vol. 4, No.1, 2026**
www.zjhms.alzahraa.edu.iq

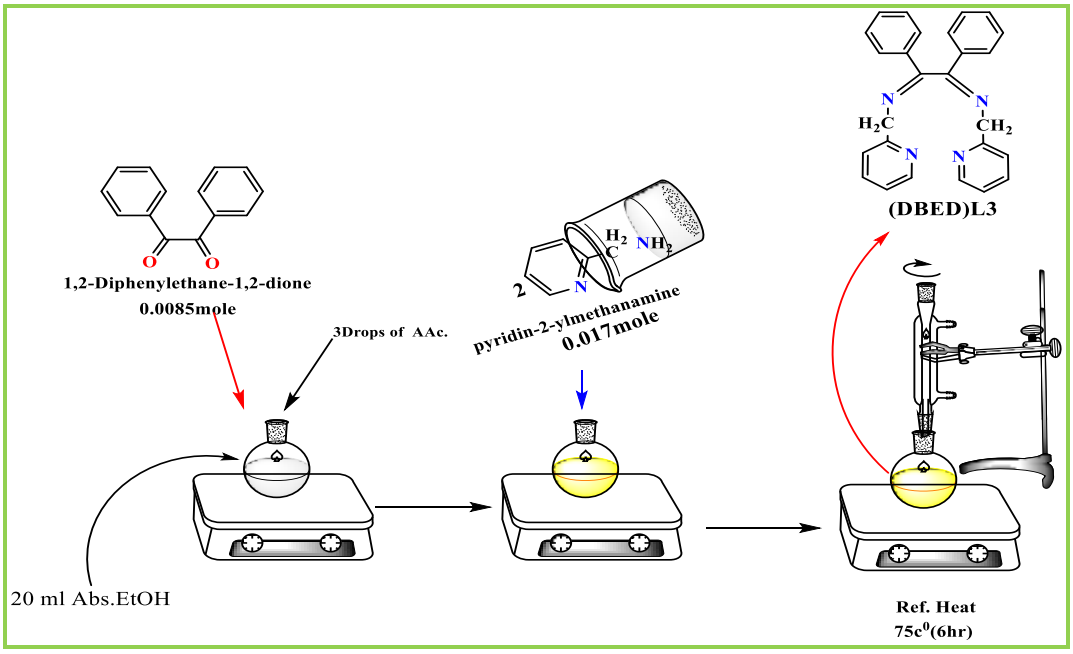

Scheme 1. The Steps of ligand (L_1) synthesis.

2.3.1 Mole Ratio Method

The absorption spectra of various mixed solutions were recorded, comprising one milliliter of the metal ion salt at the ideal concentration and differing volumes of the ligand solution at the same concentration. when these concentrations conformed to the Lambert-Beer law at the maximum wavelength (λmax), is represented by the absorption values as in Table 1. The correlation between absorbance on the Y-axis and mole ratio on the X-axis was graphed to get the (M:L) ratio. The M:L ratio is indicated by the intersection of the two linear ion complexes, which was 1:1, for the Cu(II), Ag(I), and Au(III) complexes, (M:L) metal ratio with the L_1 ligand[11]. As shown in figure1.

IRAQI Academic Scientific Journals

AL ZAHRAA UNIVERSITY JOURNAL
Health and Medical Science

*Al-Zahraa Journal for Health and Medical Sciences 2026; 4(1):*14-50 **Vol. 4, No.1, 2026**
www.zjhms.alzahraa.edu.iq

Table 1. Absorbance values for metal complex solutions at (λmax) that correspond to the ideal concentration for both the metal ion and ligand (DBED)L_1 and the molar ratio [metal: ligand]

M : L mL:mL	Absorbance of complexes at ($4.5x10^{-4}$) M and (λ_{max})		
	Cu(II) λ_{max}=690	Ag(I) λmax=410	Au(III) λmax=738
1 : 0.25	0.1	0.05	0.02
1 : 0.5	0.15	0.1	0.04
1 : 0.75	0.2	0.15	0.06
1 : 1.00	0.24	0.2	0.08
1 : 1.25	0.25	0.22	0.1
1 : 1.50	0.25	0.23	0.12
1 : 1.75	0.26	0.24	0.13
1 : 2.00	0.27	0.24	0.14
1 : 2.25	0.28	0.25	0.15
1 : 2.50	0.28	0.26	0.16
1 : 2.75	0.27	0.26	0.16
1 : 3.00	0.28	0.27	0.17

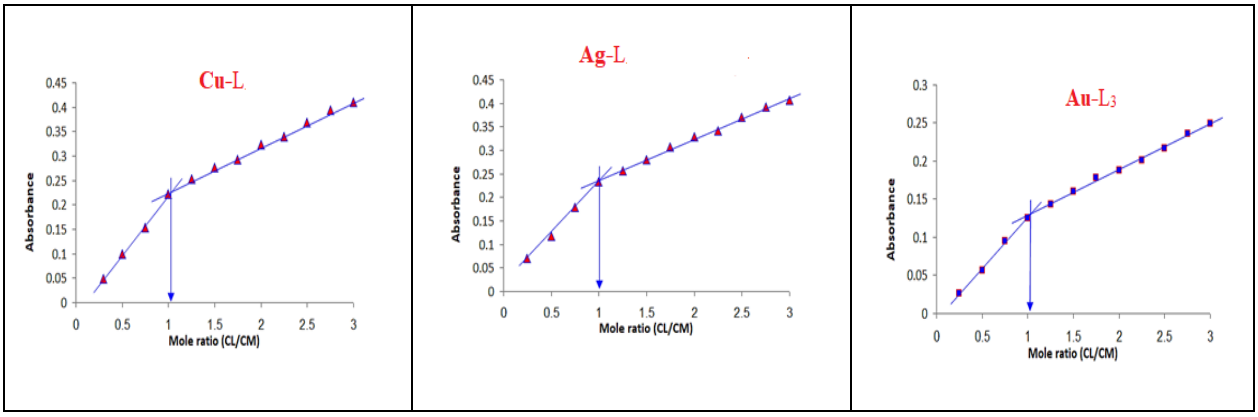

Figure 1. The molar ratio curves with (DBED)L_1ligand at (λmax) for Cu(II), Ag(I), and Au(III).

IRAQI Academic Scientific Journals

AL ZAHRAA UNIVERSITY JOURNAL
Health and Medical Science

*Al-Zahraa Journal for Health and Medical Sciences 2026; 4(1):*14-50 **Vol. 4, No.1, 2026**
www.zjhms.alzahraa.edu.iq

2.3.2 Synthesis of ligand(L_1)-Metal complexes

All novel complexes were synthesized in a mole ratio of M:L metal-to-ligand (1:1) for Cu(II), Ag(I)and Au(III) ions, and a little quantity of heated absolute ethanol was used to dissolve the (L_1) ligand (0.390g, 1 mmol) Scheme (2). The proper absolute ethanol solution of metal salts was pro-gressively supplemented with the ligand solution. The reaction mixture was heated to reflux for (90-120 minutes) and under similar working conditions in the preparation of the ligand, after the addition of $CuCl_2.2H_2O$ (0.17g, 1 mmol), $AgNO_3$ (0.1698 g, 1 mmol), and $H[AuCl_4]$ (0.339,1 mmol)[12]. After being washed with diethyl ether, the solid crude material was filtered and oven-dried, then each compound was dissolved in absolute ethanol and ultrasonically treated at a fre-quency of 20–40 kHz for 20 minutes while maintaining a temperature below 40 °C, with the aim of reducing agglomeration and improving nanodispersion without affecting the coordination structure. The compounds were then separated, washed, and dried.[13]. The different quantities of ligand as well as the per cent composition of all forming complexes are shown below in the Table 2 and Scheme 2.

Table 2. Specific physical and chemical characteristics of the Schiff base ligand (L_1) and their complexes.

No	Chemical formula	Color	M.wt g/mol	M.P°C	Yield%	Mol ratio M:L
1	L_1 (DBED) =$C_{26}H_{22}N_4$	Yellow	390.49	134-136	75	_
2	$[Cu(C_{26}H_{22}N_4Cl_2)]H_2O$	Gray	542.9	159-161	68	1:1
3	$[Au(C_{26}H_{22}N_4)]Cl_3.H_2O$	Light yellow	711.822	168-170	79	1:1
4	$[Ag(C_{26}H_{22}N_4)]NO_3$	Dark brown	560.362	148-150	69	1:1

IRAQI Academic Scientific Journals

AL ZAHRAA UNIVERSITY JOURNAL
Health and Medical Science

*Al-Zahraa Journal for Health and Medical Sciences 2026; 4(1):*14-50 **Vol. 4, No.1, 2026**
www.zjhms.alzahraa.edu.iq

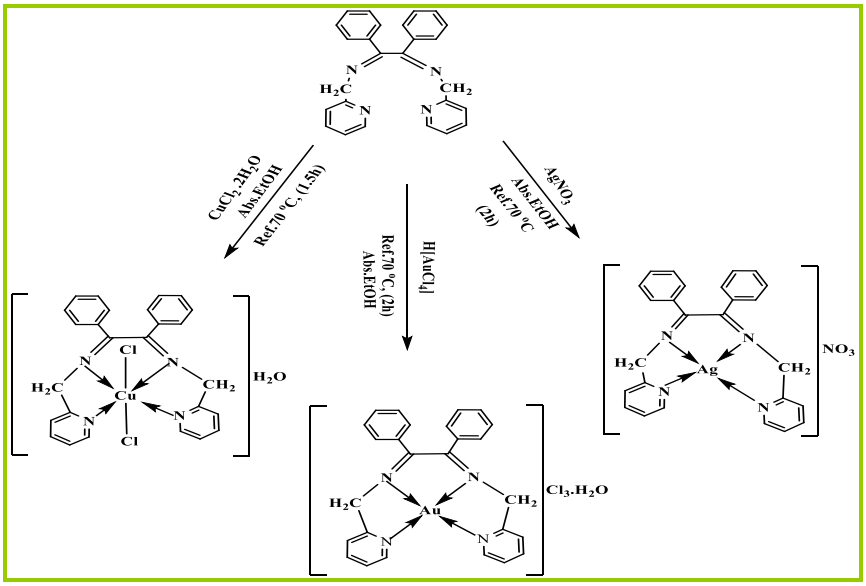

Scheme 2. Synthesis of ligand(L_1)-complexes.

2.4 Antimicrobial , Cell cytotoxicity(In Vitro Cytotoxicity) and viability Study

All recently synthesized ligands and complexes were evaluated for their antibacterial efficacy against *Staphylococcus aureus* (a gram-positive bacterium) and *Escherichia. coli* (a gram-negative bacterium) via the agar diffusion method. All chemicals demonstrated an ability to combat germs. Mueller-Hinton broth served as the medium for cultivating the test organisms. Dimethyl sulfoxide (DMSO) at a concentration of $1x10^{-3}$ M served as the solvent for chemical solutions designated for biological research. The plates were incubated at 37°C for 24 hours. The antibacterial efficiency of the synthesized compounds was assessed by measuring the diameter of the inhibitory zone produced against the corresponding test microorganism. The volume of the growth restriction area for each sample was determined by averaging three distinct replicates to reach a conclusion[8]. The PC-3, acquired from the Pastor Institute in Iran, was employed in this study, and cancer cells were cultured and examined at the University of Tehran. Cell proliferation and vitality were assessed with the MTT [3-(4, 5-dimethylthiazol-2-yl)-2, 5-diphenyltetrazolium Bromide]test for the viability of prostate cancer cells upon achieving a monolayer, the cells were exposed to 300-3.7 µg/mL of the ligand (L_1) and its Au(III)-complex to their efficacy assessment against growth prostate cancer cells (PC-3) and healthy cells(HDF). The concentration of the compounds that resulted in 50% of cell death (IC_{50}) was determined from respective dose-response curves [4].

AL ZAHRAA UNIVERSITY JOURNAL
Health and Medical Science

*Al-Zahraa Journal for Health and Medical Sciences 2026; 4(1):*14-50 **Vol. 4, No.1, 2026**
www.zjhms.alzahraa.edu.iq

3. Results and Discussion

The analysis of the ligand (L_1) and its associated metal ions is described in detail**:**

3.1 Physical characteristics and elemental examination

The ligand used in this study (L_1) is yellow in color. This ligand redeems the used metal ions to give a compound different colures in their crystallization process. Regarding the reaction with air, none of the compounds are affected since they are not soluble in water. However, they are soluble in organic solvents such as methanol, ethanol, diethyl ether, acetone, hexane ,carbon tetrachloride. Physical characteristics and the elemental analysis (C.H.N.O) analyses of the compound are presented in Table 3 besides the metallic constituents in the organized compounds. The obtained investigative data is sufficient for the investigated values of the intended magnitudes, where the complexes analytical data are well matched with the obtained experimental results data.

Table 3. Elemental analysis of (L_1) and their metal complexes

No	Chemical formula	M.wt g/mol	Element analysis found (calc.)%				
			C	H	N	O	M
1	L_1 (DBED)=$C_{26}H_{22}N_4$	390.49	Th.79.97 Ex.(80.11)	5.63 (5.81)	14.35 (14.78)	_	_
2	$[Cu(C_{26}H_{22}N_4Cl_2)]H_2O$	542.90	57.52 (57.45)	4.46 (4.55)	10.32 (10.17)	2.95 (2.73)	11.70 (12.03)
3	$[Ag(C_{26}H_{22}N_4)]NO_3$	560.36	55.73 (55.59)	3.96 (3.82)	12.50 (12.63)	8.57 (8.48)	19.25 (18.72)
4	$[Au(C_{26}H_{22}N_4)]Cl_3.H_2O$	711.82	43.87 (43.99)	3.40 (3.27)	7.87 (7.92)	2.25 (2.18)	27.67 (27.26)

Th.=theoretical value, Ex.=experimental value

AL ZAHRAA UNIVERSITY JOURNAL
Health and Medical Science

*Al-Zahraa Journal for Health and Medical Sciences 2026; 4(1):*14-50 **Vol. 4, No.1, 2026**
www.zjhms.alzahraa.edu.iq

3.2 FT-IR Spectra of Ligand (L_1) and their metal Complexes.

The complexation sites are defined via the infrared spectra of the Schiff base ligand and their complexes. Data gathered are laid out in Table 4, with some band assignments mentioned for the salient features. Figures 2 through 5 display the FT-IR spectra of the Schiff base ligand and their complexes. The spectra of the ligand exhibit the characteristic –C=N band in the region of 1630cm^{-1}attributted to the azomethine group[14],Figure2. This band is shifted to lower frequencies in the spectra of the complexes, indicating the involvement of azomethine nitrogen in bonding to the metal ions, where the bands are observed at 1617, 1622, and 1619 cm^{-1} for the Cu(II), Ag(I) and Au(III) complexes respectively[10]. The stretching vibration at 1585 cm^{-1} observed in the ligand is due to the -C=N of the picolylamine ring, and this band shifted to lower frequencies in the spectra of all the complexes, which shows that the nitrogen atom of the picolylamine ring is involved in complexation[15]. Further, the aromatic υ(C-H) vibration occurs at 3082 ,3059 ,3024 cm^{-1} in the free ligand and these frequencies get very slight change in energy and shape in all the spectra of the complexes[16]. The bands at 3429 cm^{-1} in the Cu-complex and at 3527 cm^{-1} in the Au-complex correspond to the presence of crystallization water. The assignments mentioned above are confirmed by medium intensity bands appearing in the region 545-507 cm^{-1} which have been assigned to (M-N) modes respectively[12]. These bands are not found in the spectrum of free ligand.

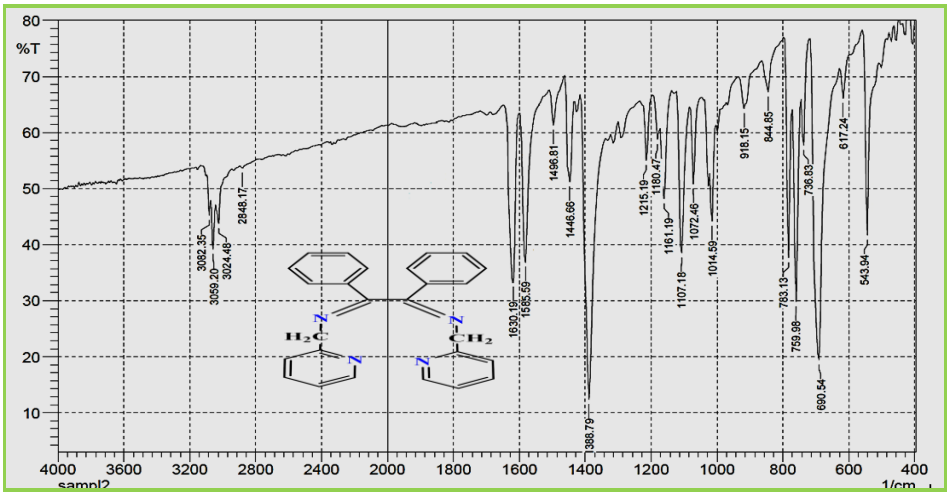

Figure2. FT-IR spectrum for (L_1).

IRAQI Academic Scientific Journals

AL ZAHRAA UNIVERSITY JOURNAL
Health and Medical Science

*Al-Zahraa Journal for Health and Medical Sciences 2026; 4(1):*14-50 **Vol. 4, No.1, 2026**
www.zjhms.alzahraa.edu.iq

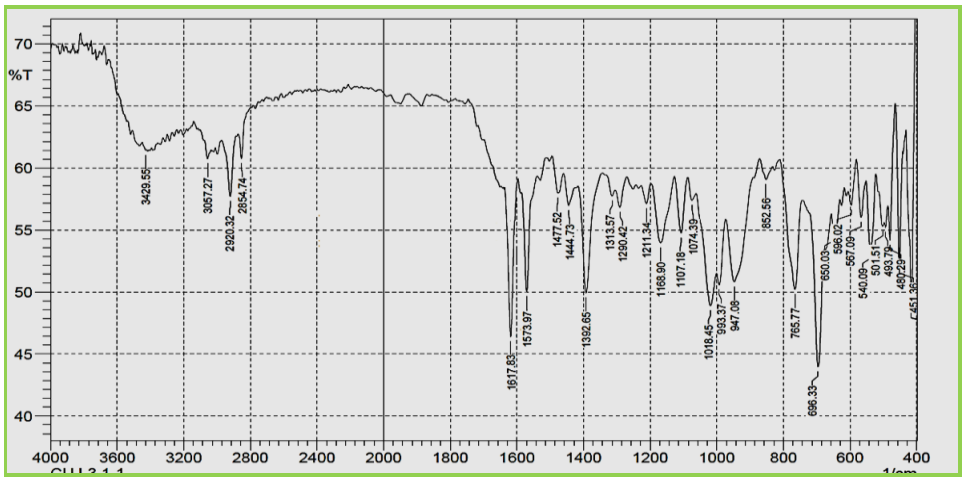

Figure 3. FT-IR spectrum for Cu-L_1.

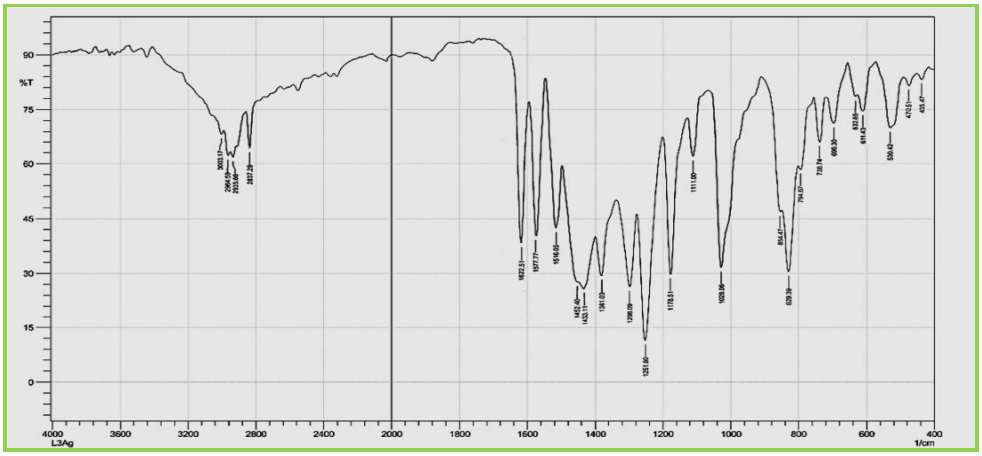

Figure 4 . FT-IR spectrum for Ag-L_1.

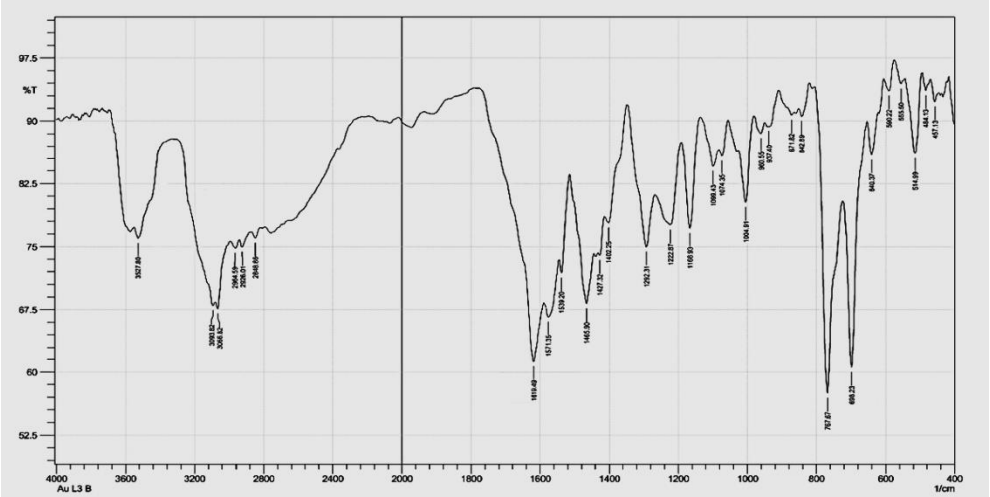

Figure 5. FT-IR spectrum for Au-L_1.

IRAQI Academic Scientific Journals

AL ZAHRAA UNIVERSITY JOURNAL
Health and Medical Science

*Al-Zahraa Journal for Health and Medical Sciences 2026; 4(1):*14-50 **Vol. 4, No.1, 2026**
www.zjhms.alzahraa.edu.iq

Table 4. FT-IR spectra of the (L_1) and their complexes (υ in cm^{-1}).

No	Chemical formula	υ (C=N) Imine	υ (C=N) Pyr.ring	υ (O-H) Hydrate	δH_2O Bend.	υ (M-N)
1	(L_1) =$C_{26}H_{22}N_4$	1630	1585.59	_	_	_
2	[Cu($C_{26}H_{22}N_4Cl_2$)]H_2O	1617	1573.97	3429	852	501-493
3	[Ag($C_{26}H_{22}N_4$)]NO_3	1622	1577.37	_	_	530-470
4	[Au($C_{26}H_{22}N_4$)]$Cl_3.H_2O$	1619	1571.35	3527	842	514-488

3.3 Electronic spectra of ligand (L_1)and their complexes

The electronic spectral data for the free Schiff base ligand (L_1) and their complexes of Cu(II), Ag(I) and Au(III) were recorded in absolute ethanol($1X10^{-4}$M) as solvent in the range of 200-800 nm at room temperature using the same solvent as blank which are shown in Figure 6 and their assignment are given in Table 5. The initial high intensity absorption peak in the electronic spectra of L_1 in ethanol was located at (235 nm, 42553 cm^{-1}), and (280 nm, 35714cm^{-1}), were attributed to the (π→π*) transitions in chromophore groups . The n→π* transitions of the nonbonding electrons in the nitrogen of the azomethine group and other oxochrom groups in the Schiff base ligand are responsible for the absorption band about (420 nm, 23809 cm^{-1})[17]. When complexation occurs, the band shift to the higher wave length region, for all of the metal Cu(II) Ag(I) and Au(III) ions core complexes. This suggests that the energy required for a certain electron transition is decrease systematically. A growing energy difference between the pertinent molecular orbitals usually the metals d-orbitals or charge-transfer orbitals in each complex causes the blue shift or higher wave number[18]. The $^2B_1g→^2B_2g$ and $^2B_1g→^2A_2g$ transitions Figure 6, was attributed to the absorption wide band seen in the Cu (II) complex at (690-760) nm(14492-13157)cm^{-1}. That was effective for distortion octahedral structures. as well as the magnetic moment value of 1.78 B.M[15]. Ag(I) complex spectrum in electronic form the Figures 6 show in the UV-vis absorption spectra of the ligands, the (π→π*) transitions of the aromatic rings are responsible for bands in the (235nm,42553cm^{-1}) region. The powerful bands at (400 nm, 25000cm^{-1}) are caused by the azomethine group (n→π*) transitions. The Ag(1) complex spectra show these bands red-shifted to the (430nm,23255 cm^{-1}) region, indicating that the

IRAQI Academic Scientific Journals

AL ZAHRAA UNIVERSITY JOURNAL
Health and Medical Science

*Al-Zahraa Journal for Health and Medical Sciences 2026; 4(1):*14-50 **Vol. 4, No.1, 2026**
www.zjhms.alzahraa.edu.iq

azomethine group is either assigned to the dπ(Ag)$^{+1}$→ π*(L)(C.T) transition or involved in coordination. The electronic spectrum data for the Ag(I) complex shows that it is diamagnetic and has a tetrahedral structure[19]. According to the Au(III) complex electronic spectra, which is displayed in Figure 6, the $^1A_1g \rightarrow {}^1A_2g$ (υ_1) transition was linked to a band at (748 nm,13368 cm^{-1}), the $^1A_1g \rightarrow {}^1B_1g$ (υ_2) transition refer to a band at (700 nm,14285 cm^{-1}), and the $^1A_1g \rightarrow {}^1Eg$ (υ_3) transition to a band at (500 nm,20000cm^{-1}). The coordination of azomethine nitrogen was also indicated by the band at (390 nm , 25641cm^{-1}) shifting to the higher wave length region, whilst the intra-ligand transition was linked to the two bands at (325 nm , 30769 cm^{-1}) and (240 nm , 41666cm^{-1}). According to the study, the Au(III) complex possesses a square planer shape and is diamagnetic[20]. The metal complexes Cu(II), Ag(I), and Au(III) showed distinct and vivid colors, indicating the coordination process between the ligand and the generated metal complex. Table 5 displays the main electronic transitions of the ligand (L_1) and their metal complexes.

Table 5. Electronic spectra, magnetic measurements, geometries and hybridization of metal complexes of ligand (L_1) under study at laboratory temperature.

Compounds	λ_{max} (nm)	Absorption Bands (cm^{-1})	Transitions	μ_{eff} (B.M)	Geometry	Hybridization
L_1	420	23809	n →π*	–	–	–
	280	35714	π →π*			
	235	42553				
Cu(II)-Complex	690-760	14492-13157	$^2E_2g \rightarrow {}^2T_2g$	1.78	Octahedral (Distorted) (Z-out)	sp^3d^2 High spin
	340	29411	n →π*			
	265	37735	π →π*			
	240	41666	π →π*			
Ag(I)-Complex	430	23255	dπ(Ag)$^{+1}$→ π*(L)(C.T)	Diama-gnetic	Tetrahedral	sp^3 Low spin
	400	25000	n →π*			
	235	42553	π →π*			
Au(III)-Complex	748	13368	$^1A_1g \rightarrow {}^1A_2g$	Diama-gnetic	Square Planer	dsp^2 Low spin
	700	14285	$^1A_1g \rightarrow {}^1B_1g$			
	500	20000	$^1A_1g \rightarrow {}^1Eg$			
	390	25641	Intra-ligand			
	325	30769				
	240	41666				

AL ZAHRAA UNIVERSITY JOURNAL
Health and Medical Science

*Al-Zahraa Journal for Health and Medical Sciences 2026; 4(1):*14-50 **Vol. 4, No.1, 2026**
www.zjhms.alzahraa.edu.iq

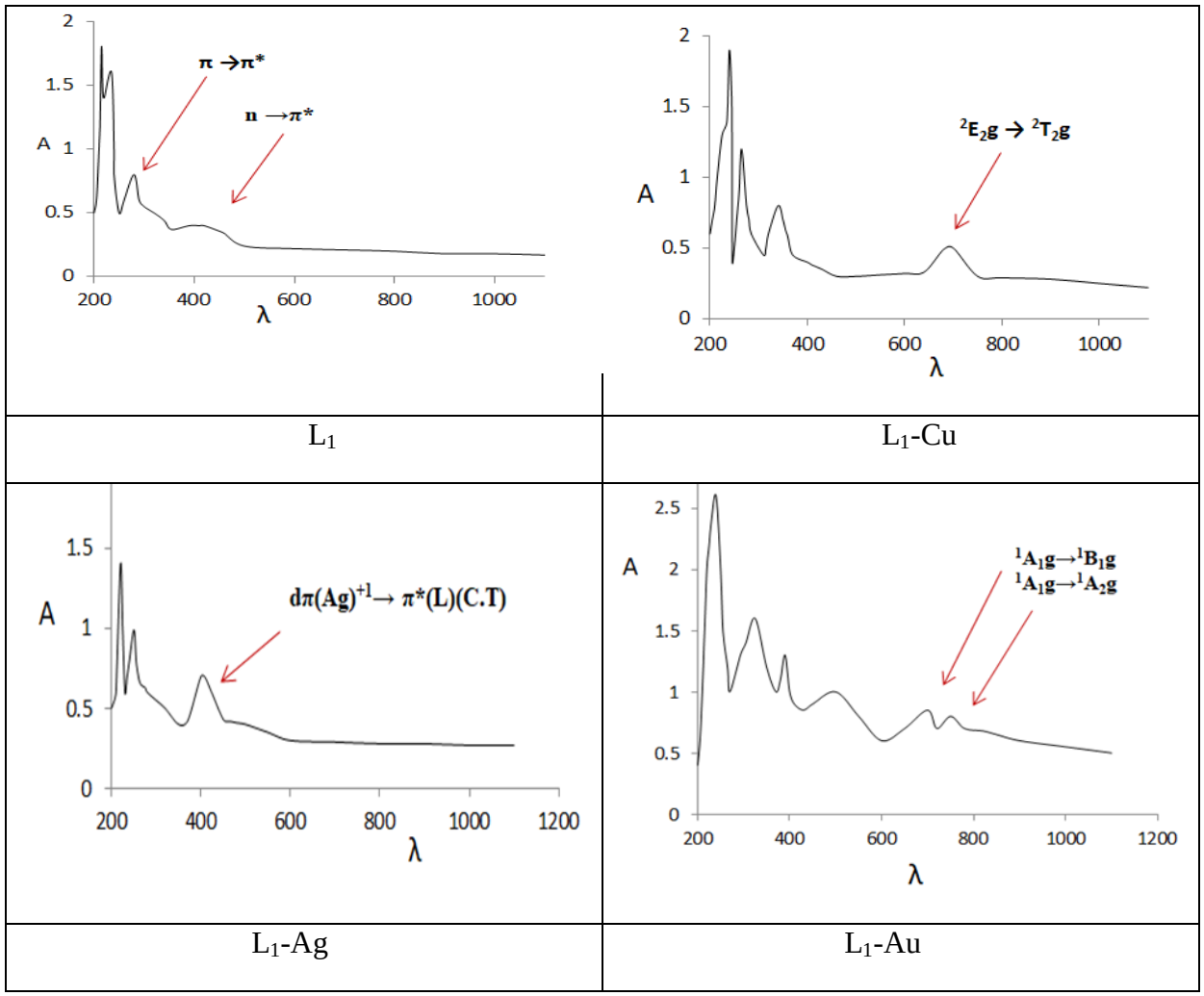

Figure 6. Ultraviolet-Visible spectra of ligand (L_1) and their metal complexes.

3.4 Conductivity measurements

Using absolute ethanol as a solvent, the molar conductivity of the metal complexes under investigation was investigated at room temperature. Table 6, which displays the results of the analysis, the conducting nature of the metal complexes with ligand L_1, were found to be 1:3 , with gold (III) while silver (I)complex have 1:1 ratio, and the value for copper(II) complex were found to be non-ionic metal complex[20].

IRAQI Academic Scientific Journals

AL ZAHRAA UNIVERSITY JOURNAL
Health and Medical Science

*Al-Zahraa Journal for Health and Medical Sciences 2026; 4(1):*14-50 **Vol. 4, No.1, 2026**
www.zjhms.alzahraa.edu.iq

Table 6. Molar conductivity values (mΛ) for ligand L_1 in solid metal complexes solutions in absolute ethanol at ambient temperature and at a concentration of (1×10^{-3}).

Metal Complexes	Molar conductivity $S.cm^2.mol^{-1}$	Electrolyte nature
$[Cu(C_{26}H_{22}N_4Cl_2)]H_2O$	9.84	Non
$[Ag(C_{26}H_{22}N_4)]NO_3$	30.13	Ionic
$[Au(C_{26}H_{22}N_4)]Cl_3.H_2O$	118.84	Ionic

3.5 ^{1}H-NMR Spectral Studies

The ^{1}H-NMR spectrum of ligand (L_1), Figure 7, in DMSO-d^6 showed protons signals due to the ligand symmetry. The single signal at (δ=5.16ppm, 2H) assigned to (CH_2) group, while the signal at (δ=8.34) ppm duo to (H-C=N) proton in pyridine ring . The aromatic proton were appeared at (δ=6.90-6.87) ppm and (8.34-7.31) ppm due to diphenylethane and pyridine ring protons, respectively[21]. The ^{1}H-NMR spectrum of prepared gold ion complex, Figures 8 showed chemical shifts listed below. The signal at (δ=8.33-7.38 ppm) duo to (H-C=N) pyridine ring proton and other protons in these ring. The diphenyl ethane protons were showed at (δ=7.37-6.93) ppm . The singlet signal at (δ=5.56 ppm) assigned to methylene protons (CH_2) that attached with the pyridine ring[22]. While the shift at δ=4.27 ppm due to crystallization water[23]. The changed in the NMR spectrum of the metal complexes concerning the ligand also conveys crucial information regarding the point of ligand interaction with the metal center.

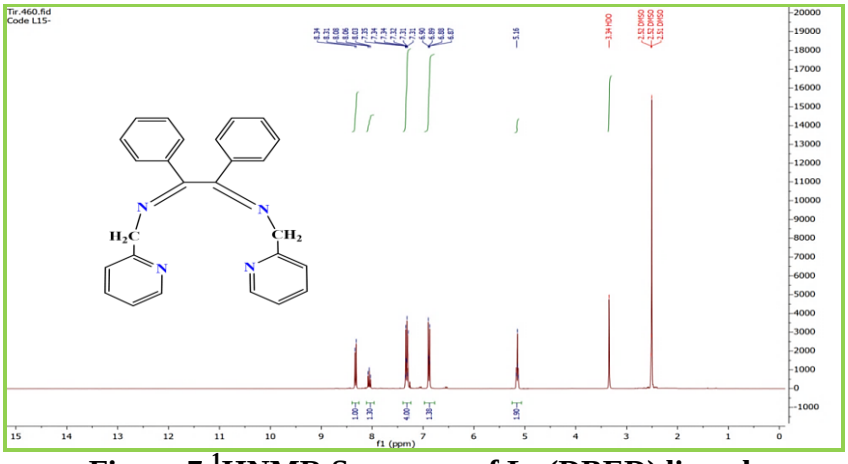

Figure 7.^{1}HNMR Spectrum of L_1 (DBED) ligand.

AL ZAHRAA UNIVERSITY JOURNAL
Health and Medical Science

*Al-Zahraa Journal for Health and Medical Sciences 2026; 4(1):*14-50 **Vol. 4, No.1, 2026**
www.zjhms.alzahraa.edu.iq

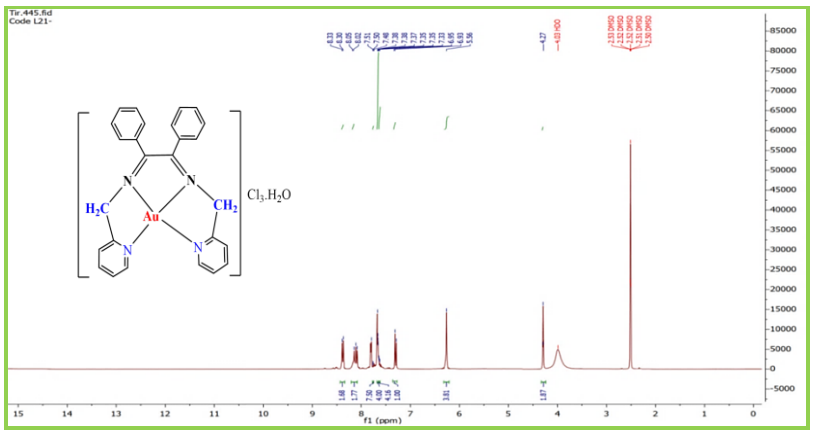

Figure8. ^{1}HNMR Spectrum of [Au(L_1)]$Cl_3.H_2O$ complex.

3.6 The Mass Spectra

Numerous previously available investigations rely on putting out the produced ligands fragmentation pathways. The mother ion peak for the $C_{26}H_{22}N_4$ ligand was found at (m+/z=390) in the mass spectrum of (L_1), Figure 9, as the parent ion peak, which was connected to the (M+) peak and is thought to be a good indication of the newly synthesized ligands. Scheme3 display the remaining pieces together with their relative abundances and fragmentation paths[24]. According to the mass spectra of the [Ag($C_{26}H_{22}N_4$)]NO_3 complex, the peaks at m/z+=560 in Figures 10 , correspond to the parent ions (M+) in the Ag-complex [25]. Scheme4 display the remaining pieces, their relative abundances, and the fragmentation paths for the above complex.

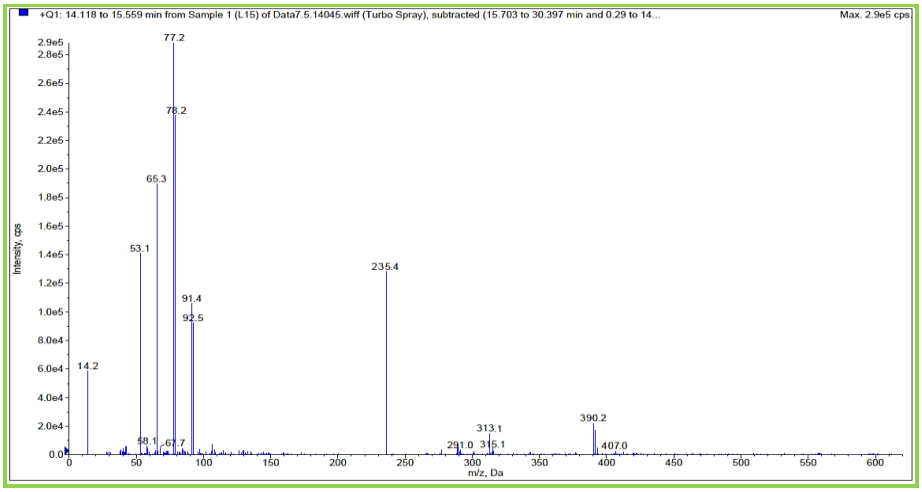

Figure 9. Mass spectrum of the (L_1) ligand.

IRAQI Academic Scientific Journals

AL ZAHRAA UNIVERSITY JOURNAL
Health and Medical Science

*Al-Zahraa Journal for Health and Medical Sciences 2026; 4(1):*14-50 **Vol. 4, No.1, 2026**
www.zjhms.alzahraa.edu.iq

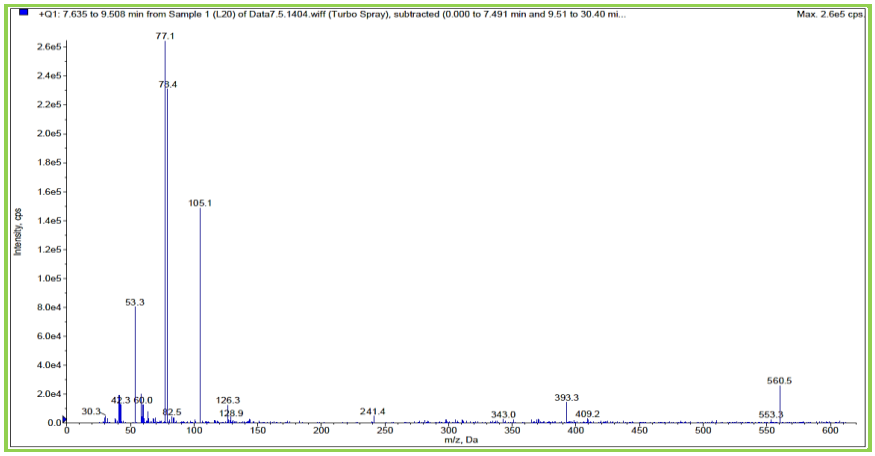

Figure10. Mass spectrum of the [Ag(L_1)]NO_3complex.

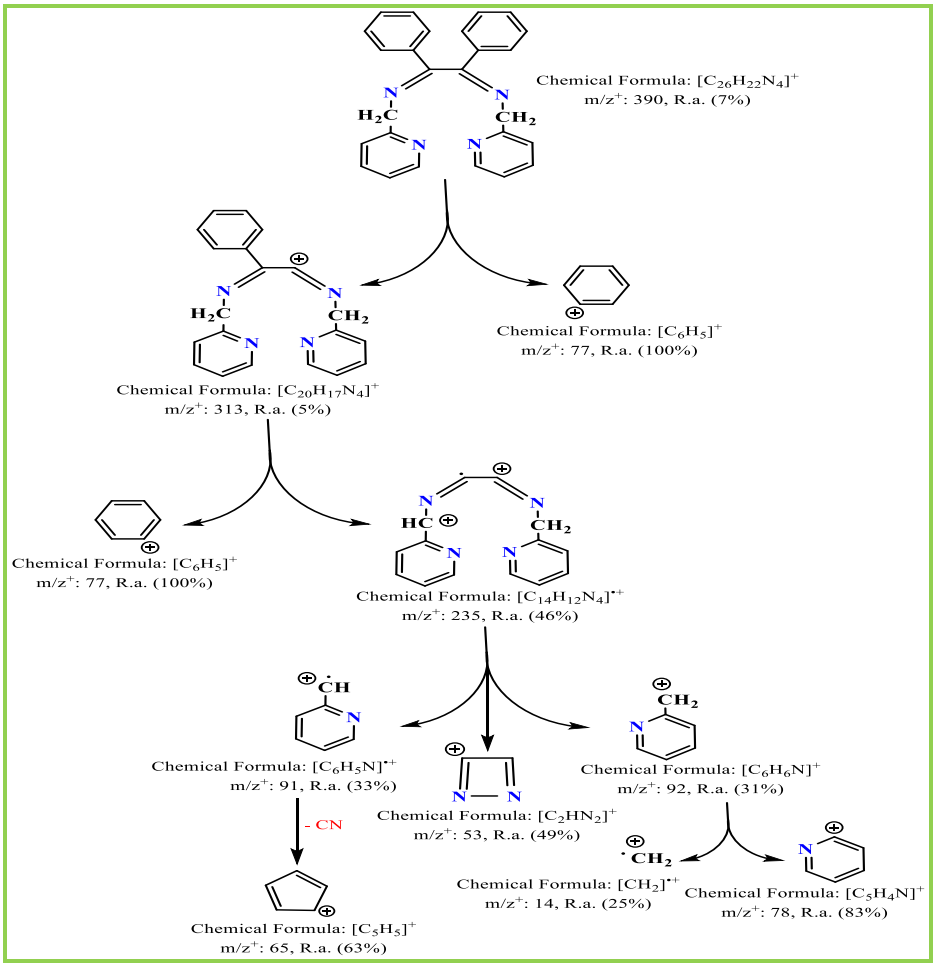

Scheme 3. The Proposed fragmentation pathways of (L_1) ligand.

IRAQI Academic Scientific Journals

AL ZAHRAA UNIVERSITY JOURNAL
Health and Medical Science

*Al-Zahraa Journal for Health and Medical Sciences 2026; 4(1):*14-50 **Vol. 4, No.1, 2026**
www.zjhms.alzahraa.edu.iq

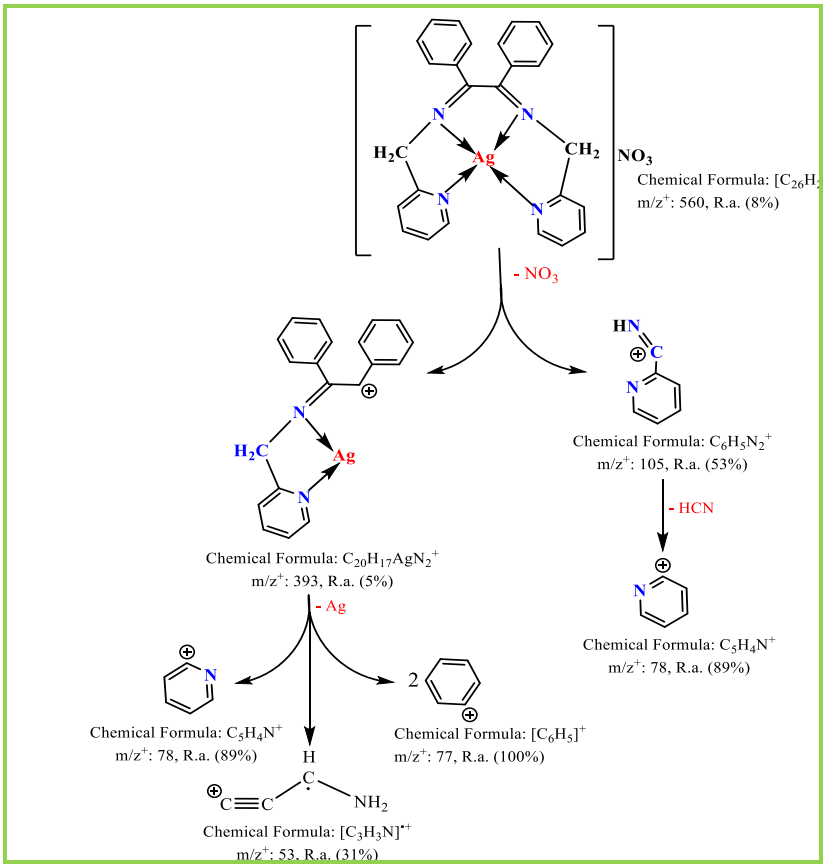

Scheme 4. The Proposed fragmentation pathways of [Ag(L_1)]NO_3complex.

3.7 X-ray diffraction study (XRD)

The ligand (L_1) and thrir metal complexes were analyzed in their solid state through X-ray diffraction within the angular range of 2(5-80°). To determine their purity and the defects that arose in the crystal structure upon the conversion of the ligands into metal complexes, micro stresses and dislocation density were calculated. The d spacing between the crystal planes for the ligand $L_1$and their metal complexes was ascertained using Bragg's law, $n\lambda = 2d \sin\theta$, where d represents the distance between the crystal planes. n is an integer. λ denotes the wave length of the X-rays, specifically CuKα = 0.1540598 Å or 1.540598 nm. Θ denotes the angle of deviation. The Scherer equation estimates the average particle size and its distribution, mathematically expressed as $D = k \lambda / \beta \cos\Theta$, where D represents the average grain size, k is Blank's constant (0.891), λ denotes the X-ray wave length (0.15405 nm), Θ is the diffraction angle, and β signifies the full width at half maximum of an observed peak [26]. Moreover, it was shown that the ligand

IRAQI Academic Scientific Journals

AL ZAHRAA UNIVERSITY JOURNAL
Health and Medical Science

*Al-Zahraa Journal for Health and Medical Sciences 2026; 4(1):*14-50 **Vol. 4, No.1, 2026**
www.zjhms.alzahraa.edu.iq

and their metal complexes under examination exhibited a grain size of less than 100 nm, categorizing them within the nanoscale range.[26] In the X-ray spectrum, Table 7 displays the diffraction angles, observed d values, relative intensity, crystal size, crystal intensity, peak widths at mid-intensity, micro-resistance, and dissolution density of the ligand L_1 and their metal complexes under study in Table 7. The X-ray diffraction spectra of the ligand L_1 and several of their metal complexes are presented in Figures from 11 to 13.

Table 7. The diffraction angles, observed d values, relative intensity, average size, peak widths at mid-intensity, and crystal dimensions for each ligand (L_1) and their complexes.

Compound	FWHM	Crystallite Size D (nm)	Dislocation density $\delta*10^{-3}$ $(nm)^2$	Micro strain $\varepsilon * 10^{-3}$	Average size (nm)
L_1=(DBED)	0.229	34.89341	0.821322	9.241364	26.54338
	0.493	16.30461	3.761657	13.95094	
	0.729	11.03992	8.204809	19.61213	
	0.633	12.7535	6.148105	15.28387	
	0.415	19.49891	2.630143	9.345255	
	0.288	28.3065	1.248038	5.456125	
	0.313	26.09616	1.468408	5.713448	
	0.197	41.55464	0.57911	3.456431	
	0.431	19.05636	2.753721	7.166098	
	0.693	12.06311	6.871975	9.229995	
Ag-complex	0.465	17.17616	3.389596	19.56024	21.17032
	0.602	13.33267	5.625559	18.2372	
	0.455	17.70538	3.189992	11.79986	
	0.55	14.69992	4.627752	12.69648	
	0.411	19.71056	2.573962	8.983286	
	0.434	18.71727	2.854402	8.870622	
	0.262	31.0794	1.035272	5.082042	
	0.553	14.81548	4.555843	9.56911	
	0.322	25.51397	1.536187	5.331612	
	0.46	17.9927	3.088925	6.867404	
	0.667	12.04138	6.896799	19.57634	

AL ZAHRAA UNIVERSITY JOURNAL
Health and Medical Science

*Al-Zahraa Journal for Health and Medical Sciences 2026; 4(1):*14-50 Vol. 4, No.1, 2026
www.zjhms.alzahraa.edu.iq

Au-complex	0.248	32.47573	0.948161	6.489358	23.01442
	0.399	20.24599	2.439619	9.443996	
	0.316	25.62162	1.523305	7.011658	
	0.329	24.67929	1.641854	6.79798	
	0.586	13.925	5.157149	10.89715	
	0.369	22.23055	2.023483	6.257191	
	0.533	15.63806	4.08916	7.324949	
	0.205	41.43615	0.582427	2.362997	
	0.437	21.85038	2.094507	2.859409	

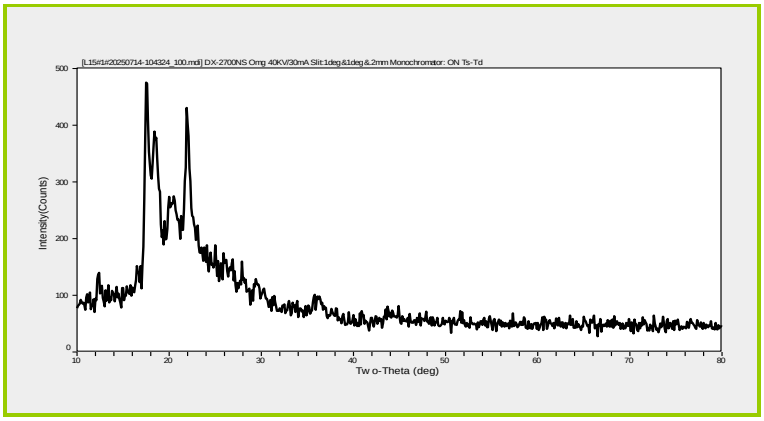

Figure 11. X-ray diffraction spectrum of the (L_1)ligand.

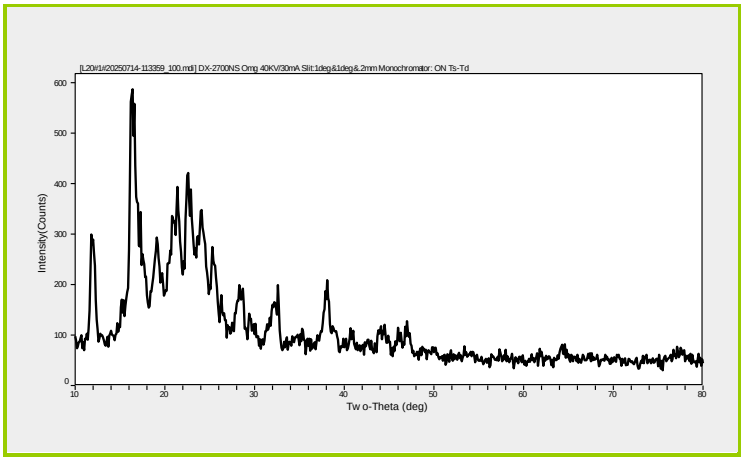

Figure12. X-ray diffraction spectrum of the [Ag(L_1)]NO_3complex.

IRAQI Academic Scientific Journals

AL ZAHRAA UNIVERSITY JOURNAL
Health and Medical Science

*Al-Zahraa Journal for Health and Medical Sciences 2026; 4(1):*14-50 **Vol. 4, No.1, 2026**
www.zjhms.alzahraa.edu.iq

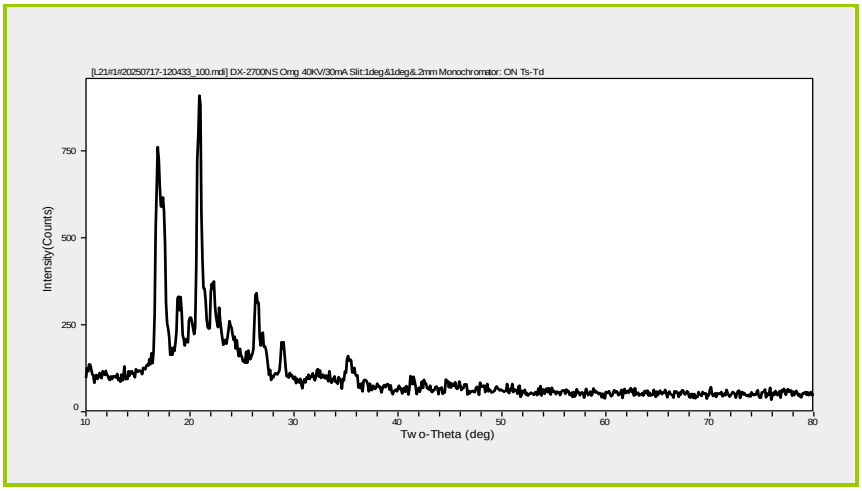

Figure13. X-ray diffraction spectrum of the [Au(L_1)]Cl_3.H_2Ocomplex.

3.8 Field-emission Scanning Electron Microscope Analyzes

The FE-SEM images provided in Figure 14 evidently confirmed that the studied ligand, L_1 and their metal complexes, have a grain size of less than 100 nanometers, referring to their nanoscale[27]. XRD examinations were carried out on average crystal size (D) calculations, showing the relative closeness, thus proving the validity of the results[28]. This characteristic possessed by the ligands and their prepared metal complexes makes these compounds useful in many fields, including in the field of biology and medicine as a curative agent to the extent to which they are suitable for eliminating many types of cancers , including prostate cancer (PC-3), and the possibility for its usage as medicine, which will be described in detail in the current study[29]. The other obtained results support our earlier measurements of X-Ray Diffraction analysis.

IRAQI Academic Scientific Journals

AL ZAHRAA UNIVERSITY JOURNAL
Health and Medical Science

*Al-Zahraa Journal for Health and Medical Sciences 2026; 4(1):*14-50 **Vol. 4, No.1, 2026**
www.zjhms.alzahraa.edu.iq

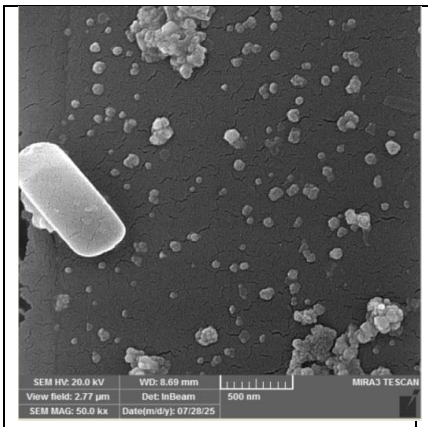

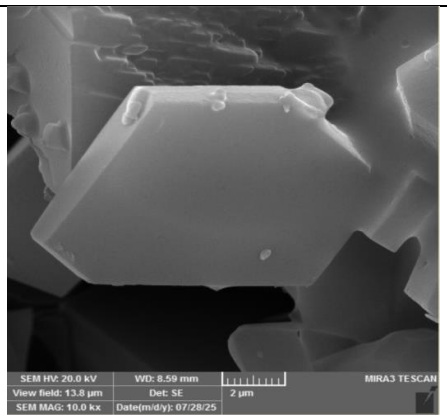

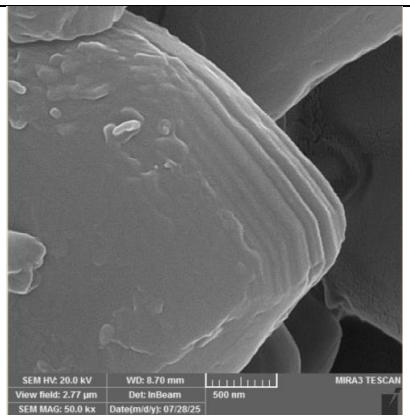

L_1-Ag	L_1-Au	$L_{1=}$ (DBED)

Figure14. Ligand (L_1) FE-SEM images of ligand and their complexes .

3.9 Proposed Molecular Structures and Geometry

Taking into account the available coordination sites in the ligands discussed in the previous literature vis-a-vis different metal ions through the spectral and analytical results obtained from diagnostic measurements based on the molar ratios and magnetic measurements, molar electrical conductivity measurements, and results from ^{1}H-NMR, mass spectroscopy, UV-Vis spectroscopy, and FT-IR, are in agreement with tetra-dentate behavior of the ligands L_1 on coordination through the nitrogen atoms within the azomethine belonging to pyridine -2-ylmethanamine and 1,2 –diphenylethane-1,2-dione rings under consideration, thus forming five-membered chelate rings which add stability to the formed metal complexes. The study results summarized in the Tables from 1 to 6 show that the coordination number of the metal ions copper(II) in their coordination complex with the ligands L_1, is hexa coordinate and thus the suggested spatial arrangement for these complexes is octahedral. The coordination number for the silver(I) ion is 4 for the ligands (L_1), with a tetrahedral shape, while for the gold(III) ion, a square planar is suggested with ligand. Regarding chloride ions often act as ligands, donating electron pairs to a central metal ion to form stable complexes, completing its coordination sphere in Cu(II), ion complex. The spatial forms proposed for the respective metal complexes being studied are illustrated in Figure 15.

IRAQI Academic Scientific Journals

AL ZAHRAA UNIVERSITY JOURNAL
Health and Medical Science

*Al-Zahraa Journal for Health and Medical Sciences 2026; 4(1):*14-50 **Vol. 4, No.1, 2026**
www.zjhms.alzahraa.edu.iq

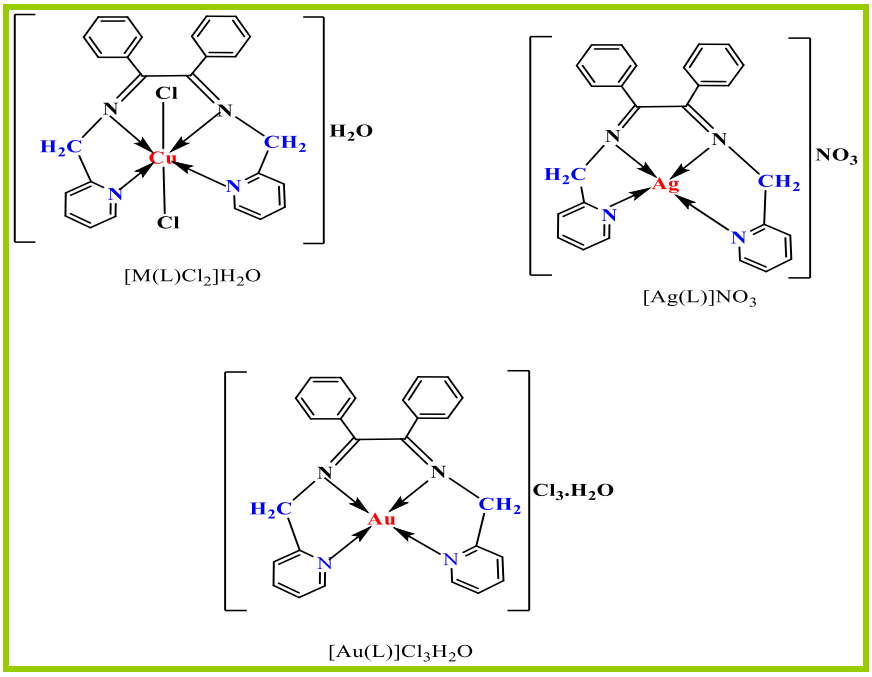

Figure 15. The proposed structural models for metal ion- L_1 complexes.

3.10 Antimicrobial activity

This study included Gram-positive bacteria *(Staphylococcus aureus)* and Gram-negative bacteria *(Escherichia coli).* The disc diffusion method was employed in this work to determine the inhibition zone in millimeters (mm). The synthesized compounds were prepared in DMSO at a concentration of 0.1 **µg** /mL, which demonstrated no inhibition of bacterial growth[30]. The inhibition values for growth, as presented in Table 8, are notably promising. The final results are illustrated in the bar graph shown in Figure 16. The results indicate that L_1-Ag and L_1-Au had more efficacy against *Staphylococcus aureus* than all other examined compounds. In comparison to the other compounds, the L_1 compound showed reduced antibacterial activity against E. coli at all dosages. According to the comparative analysis of the obtained antibacterial data, the L_1-Ag and L_1-Cu metal complexes exhibited superior inhibitory effects against E. coli. The activity data reveals that L_1 exhibit the lowest effectiveness against *Staphylococcus aureus* and *Escherichia coli.* In summary, the results indicate that each examined molecule exhibits robust antibacterial activity against all isolates, with metal complexes identified as the most effective antibacterial agents. Because their modes of actions could include inhibiting protein synthesis or rupturing

IRAQI Academic Scientific Journals

AL ZAHRAA UNIVERSITY JOURNAL
Health and Medical Science

*Al-Zahraa Journal for Health and Medical Sciences 2026; 4(1):*14-50 **Vol. 4, No.1, 2026**
www.zjhms.alzahraa.edu.iq

cell walls, the organisms eventually die. In metal complexes, the net positive charge of metal ions will be distributed over a chelate ring to decrease the polarity of the metal atoms. After chelation, such charge dispersion will be supported by the donor atoms of the ligand itself[31]. The zones of inhibition (in mm) are documented in Table 8, and Figure16 illustrates the statistical representation of antibacterial activity for ligands L_1 and their complexes. The photos in Figure17 revealed their antibacterial efficacy against two harmful microorganisms.

Table 8. Inhibition area (mm) of bacterial sensitivity to compound (area of inhibition).

Compound	**Bacteria**	
	Gram-Positive	**Gram-Negative**
	Staphylococcus aureus	***Escherichia coli***
DMSO	0	0
(L_1)	16	13
[Cu (L_1)Cl_2]H_2O	18	16
[Au(L_1)] Cl_3.H_2O	20	14
[Ag(L_1)]NO_3	20	15

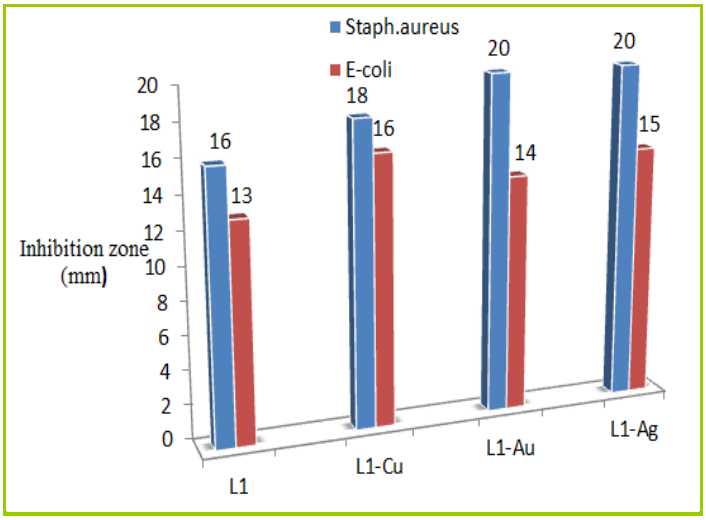

Figure 16. The statistical description of the antibacterial effectiveness of L_1 and their complexes.

AL ZAHRAA UNIVERSITY JOURNAL
Health and Medical Science

*Al-Zahraa Journal for Health and Medical Sciences 2026; 4(1):*14-50 **Vol. 4, No.1, 2026**
www.zjhms.alzahraa.edu.iq

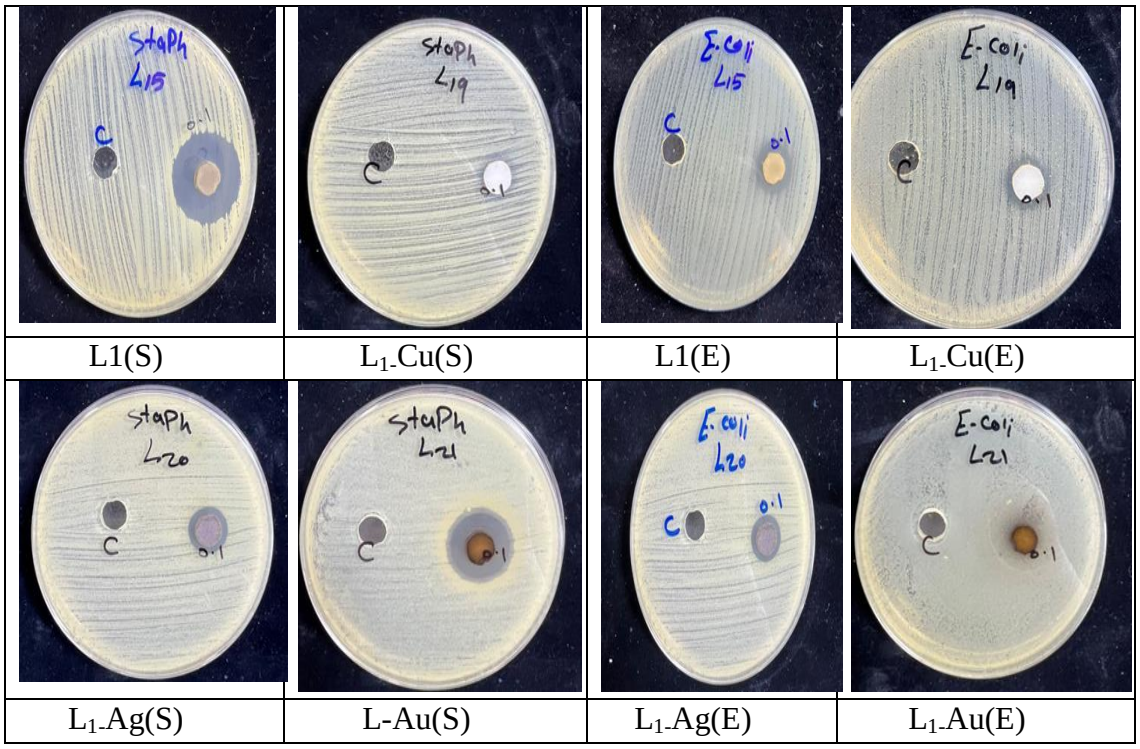

Figure17. Antibacterial activity against pathogenic bacteria with metal complexes ofL_1(DBED) Schiff base ligand, S=*Staphylococcus aureus* ,E= *Escherichia coli*.

3.11 Molecular docking

The theoretical study used the (MOE) Molecular Operating Environment program to show the molecular docking mechanism of the ligand (L_1) Schiff base and their complexes $[Au(L_1)]Cl_3.H_2O$ with prostate PC-3 cancer protein (4EJN). Following molecular docking with the 4EJN protein, the two compounds showed strong binding affinities with varying degrees of stability in the active pocket. The strongest binding, −10.6678 kcal/mol, was achieved with the standard ligand, indicating a stable and well-fitted complex inside the receptor cavity. The other two compounds had less negative values, indicating weaker but still favorable binding interactions[32].

3.11.1 Docking results for L_1

Compound L_1(pose1) exhibited lower binding affinities, extending −7.108 kcal/mol, which nevertheless reflect acceptable docking scores but had smaller hydrogen bonding networks. Less stable docking orientations resulted from these ligands primary reliance on weaker H-bond or π–

IRAQI Academic Scientific Journals

AL ZAHRAA UNIVERSITY JOURNAL
Health and Medical Science

*Al-Zahraa Journal for Health and Medical Sciences 2026; 4(1):*14-50 Vol. 4, No.1, 2026
www.zjhms.alzahraa.edu.iq

H interactions with Ile84 and Cys310[31], as seen as in table 9 and Figure18.

Table 9. Information of the best poses of ligand L_1 with protein 4EJN.

Compounds	Binding Affinity Kcal/mol	Rmsd (Å)	Atom of compound	Atom of Receptor	Involved receptor residues	Type of interaction bond	Distance (Å)	E (kcal/mol)
5- pose1	-7.10872	1.673909	N 22	O	HOH 752	(A) H-acceptor	3.07	-1
			6-ring	CG2	ILE 84	(A) pi-H	4.27	-0.6
			6-ring	CB	CYS 310	(A) pi-H	4.22	-0.4
			6-ring	CB	CYS 310	(A) pi-H	4.24	-0.4

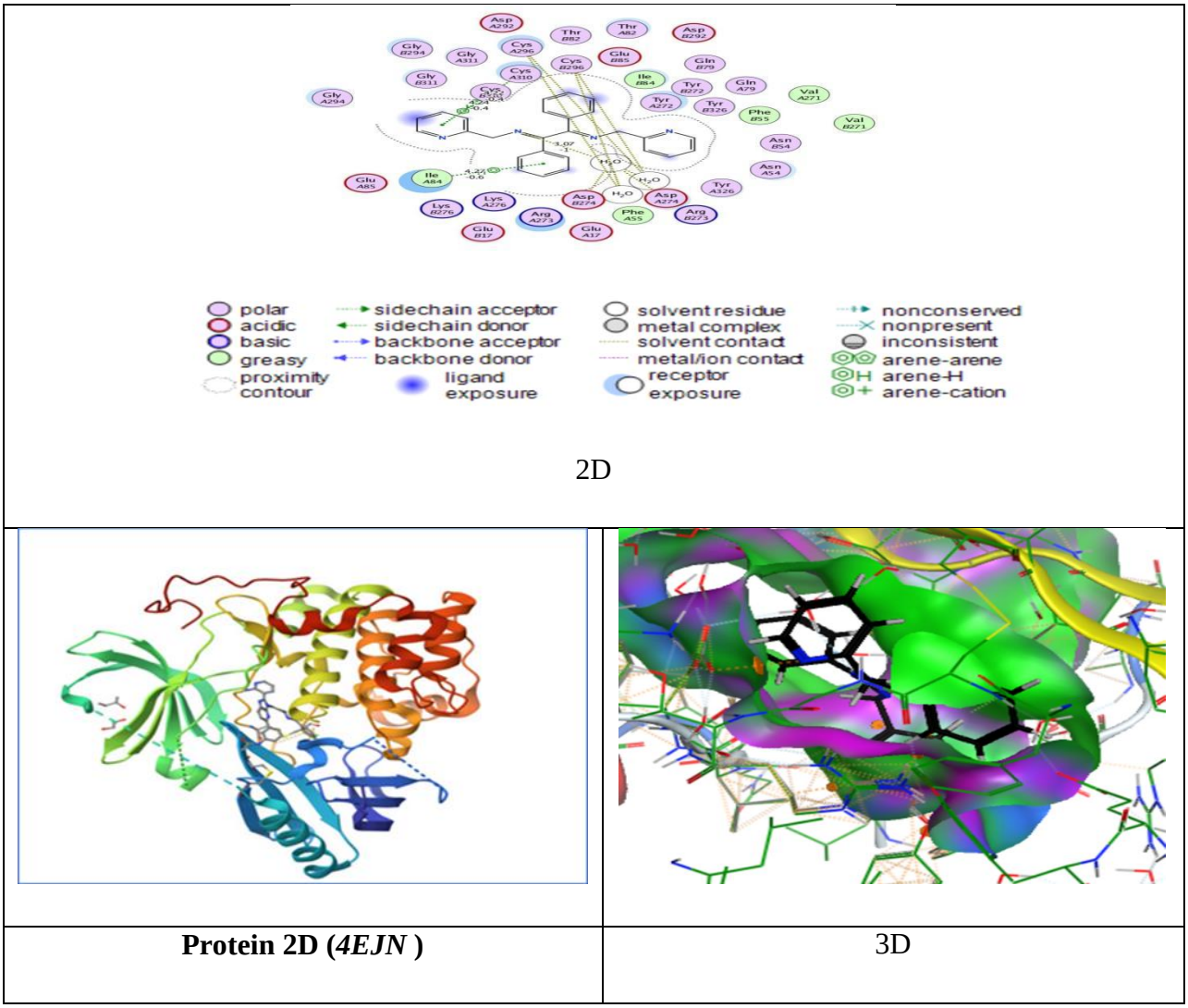

Figure18. 2D and 3D images, of the interaction between the ligand L_1 and the protein (4EJN).

IRAQI Academic Scientific Journals

AL ZAHRAA UNIVERSITY JOURNAL
Health and Medical Science

*Al-Zahraa Journal for Health and Medical Sciences 2026; 4(1):*14-50 **Vol. 4, No.1, 2026**
www.zjhms.alzahraa.edu.iq

3.11.2 Docking results for $[Au(L_1)]Cl_3.H_2O$

In compound $[Au(L_1)]Cl_3.H_2O$ (pose1) had lower binding affinities, vacillate at -7.323kcal/mol, which nevertheless reflect acceptable docking scores but have smaller hydrogen bonding networks. These ligands produced fewer stable docking orientations because they primarily depended on weaker H-bond or π–H interactions with Trp80,Val270 , These combined polar and non-polar interactions make compound Au-$L_1$the most promising candidate, closely approaching the binding efficiency of the standard drug. This good binding mode with protein(4EJN) support its potent inhibitory activity with IC_{50} =51.48 µg/mL [33]the studied compound Au-L_1 are shown in Table 10 and Figure19.

Table 10. Information of the best poses of $[Au(L_1)]Cl_3.H_2O$complex with protein 4EJN.

Compounds	Binding Affinity Kcal/mol	Rmsd (Å)	Atom of compound	Atom of Receptor	Involved receptor residues	Type of interaction bond	Distance (Å)	E (kcal/mol)
6- pose1	-7.32375	1.579417	N 3 6-ring 6-ring 6-ring 6-ring 6-ring	O CB CG2 CB CG1 CG2	HOH 679 TRP 80 VAL 270 TRP 80 VAL 270 VAL 270	(A) H-donor (A) pi-H (A) pi-H (A) pi-H (A) pi-H (A) pi-H	3.33 3.85 3.64 3.82 4.47 3.68	-0.3 -0.2 -0.3 -0.3 -0.3 -0.5

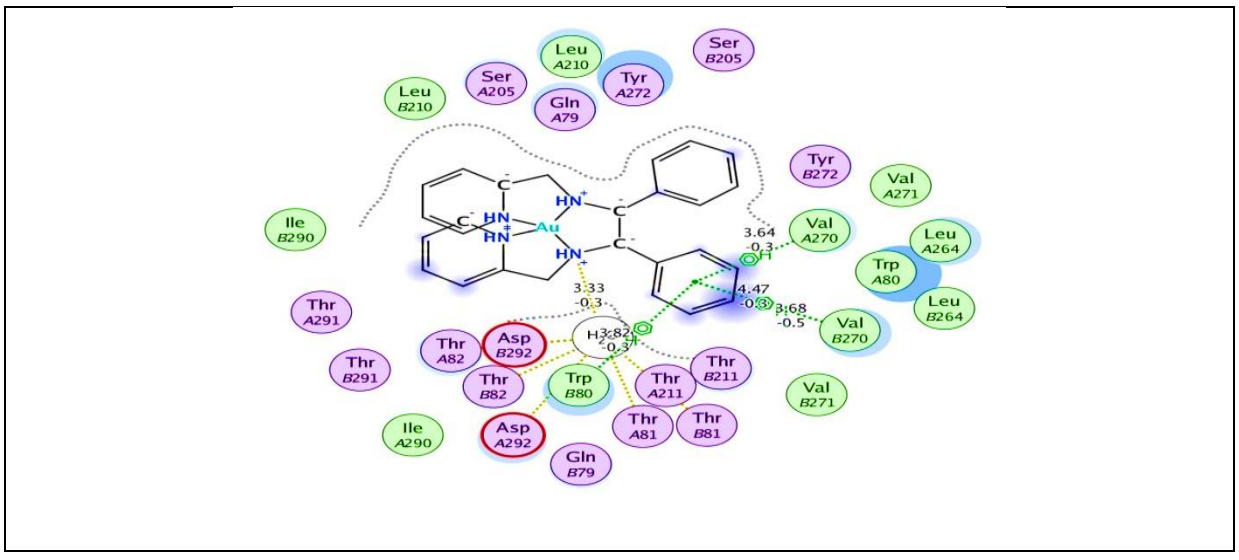

AL ZAHRAA UNIVERSITY JOURNAL
Health and Medical Science

*Al-Zahraa Journal for Health and Medical Sciences 2026; 4(1):*14-50 **Vol. 4, No.1, 2026**
www.zjhms.alzahraa.edu.iq

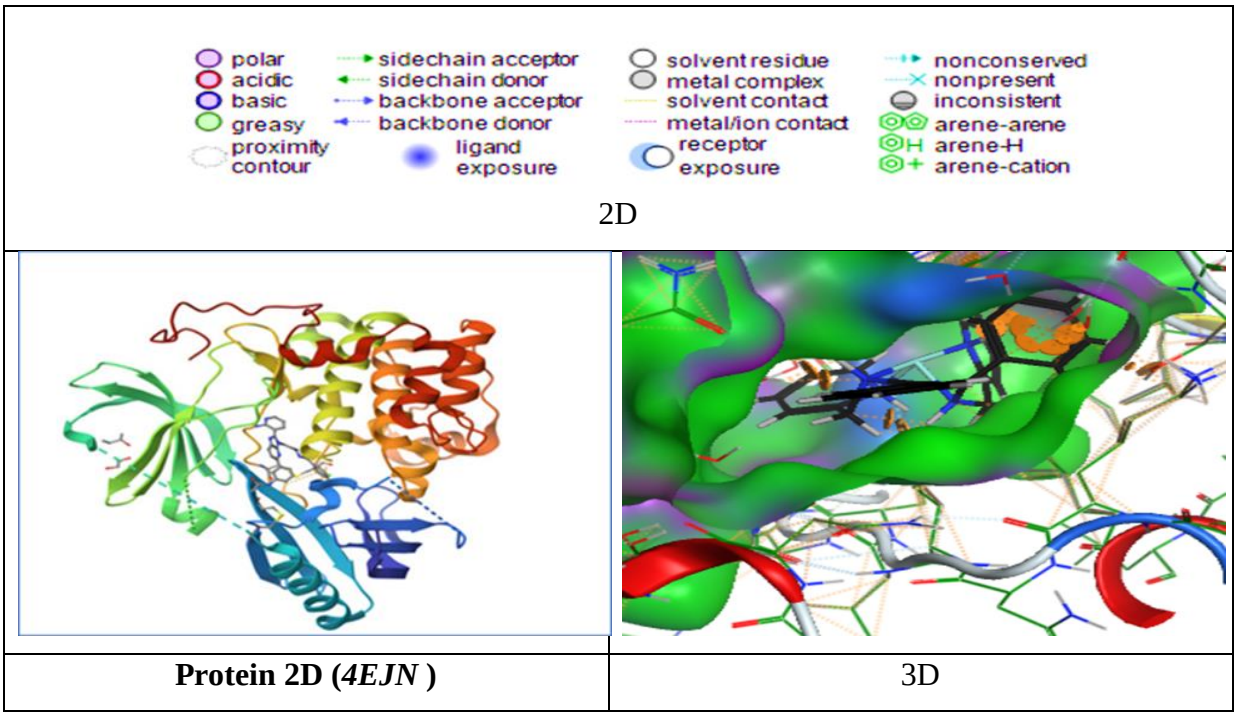

Figure 19. 2D and 3D images, of the interaction between the $[Au(L_1)]Cl_3.H_2O$ complex and the protein (4EJN).

4. Effect of ligand(L_1) and $[Au(L_1)]Cl_3.H_2O$ on growth of (PC-3) and Healthy cells (HDF):

The ligand L_1 and its gold(III) complex **$[Au(L_1)]Cl_3.H_2O$** were tested for anticancer activity against the prostate cancer cell line PC-3 and safety against the normal prostate cell line HDF. New bioactive compounds with selective cytotoxicity are essential for cancer treatment. measured cell viability and anticancer activity of these compounds against PC-3 cells at five concentrations using the MTT assay[10]. The results showed that L_1 strongly inhibited cancer cells. The strongest PC-3 cell growth inhibition occurred at the highest concentration (300 µg/mL). L_1 and its gold(III) complex inhibited growth by 62.38% and 64.20 % at this dose. At the lowest concentration (3.7 µg/mL), the PC-3 cell line showed minimal inhibition, with rates of 17.19% and 10.80%, respectively. The half-maximal inhibitory concentration (IC_{50}) values confirmed selective toxicity. The IC_{50} values for PC-3 cancer cells were 71.49 µg/mL for L_1 and 51.48 µg/mL for gold(III) complex. Normal HDF cells had IC_{50} values of 2639.22 µg/mL and 817.24 µg/mL, respectively. These results suggest that the gold(III) complex selectively harms prostate cancer cells over normal cells, supporting its potential as a novel anticancer therapy. Tables 11 and 12 and Figures 20 into 27 show the dose-dependent effects on PC-3 cancer cells

AL ZAHRAA UNIVERSITY JOURNAL
Health and Medical Science

*Al-Zahraa Journal for Health and Medical Sciences 2026; 4(1):*14-50 Vol. 4, No.1, 2026
www.zjhms.alzahraa.edu.iq

compared to HDF normal cells using the 24-hour MTT assay at 37°C.

Table 11. The proliferation inhibition effects of the ligand (L_1) by the MTT test for 24 hours on a prostate cancer cell line (PC-3) and compares it to the normal cell line (HDF) for the same concentration.

Con. (µg/mL)	Mean Percentage (%) for each cell line					
	PC-3			HDF		
	Cancerous line cells of PC-3			Normal line cells of HDF		
	Cell Viability%	SD	Cell Inhibition %	Cell Viability%	SD	Cell Inhibition%
3.7	82.81	8.34	17.19	95.00	6.08	5.00
11.11	63.79	8.93	36.21	90.47	4.28	9.53
33.33	60.88	1.76	39.12	77.79	2.8	22.21
100	43.44	6.70	56.56	69.53	5.59	30.47
300	37.62	1.06	62.38	67.79	1.48	32.21
IC_{50}= 71.49 µg/mL				**IC_{50}=2693.22 µg/mL**		

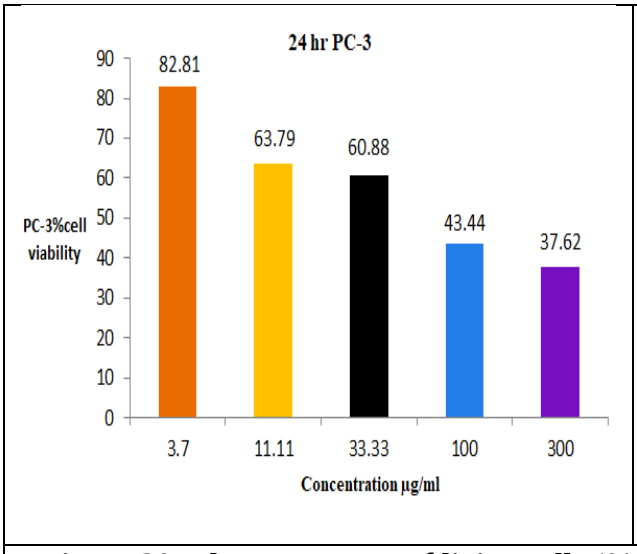

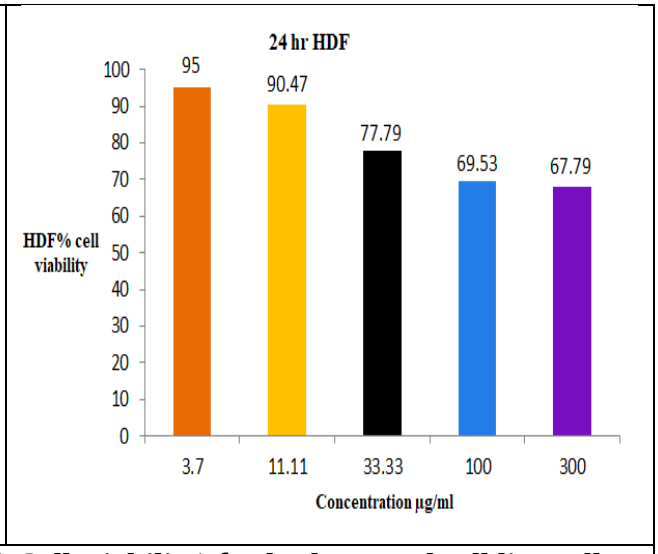

Figure 20. The percentage of living cells (% Cell Viability) for both normal cell line cells (HDF) and prostate cancer cell lines (PC-3) in relation to the ligand concentration (L_1).

IRAQI Academic Scientific Journals

AL ZAHRAA UNIVERSITY JOURNAL
Health and Medical Science

*Al-Zahraa Journal for Health and Medical Sciences 2026; 4(1):*14-50 **Vol. 4, No.1, 2026**
www.zjhms.alzahraa.edu.iq

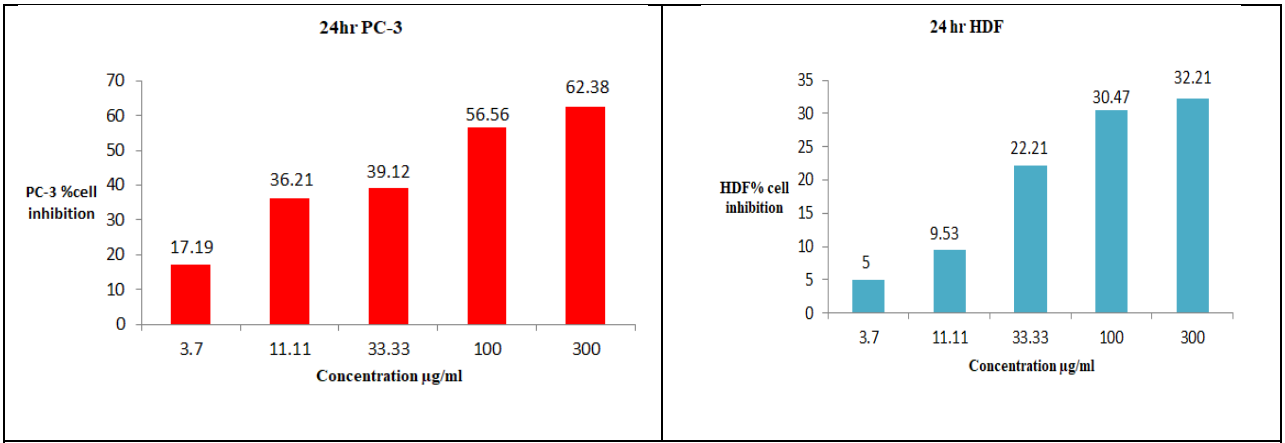

Figure 21:The percentage of inhibition (% Inhibition) of the ligand (L_1) on normal cell lines (HDF) and prostate cancer cell lines (PC-3) at several doses.

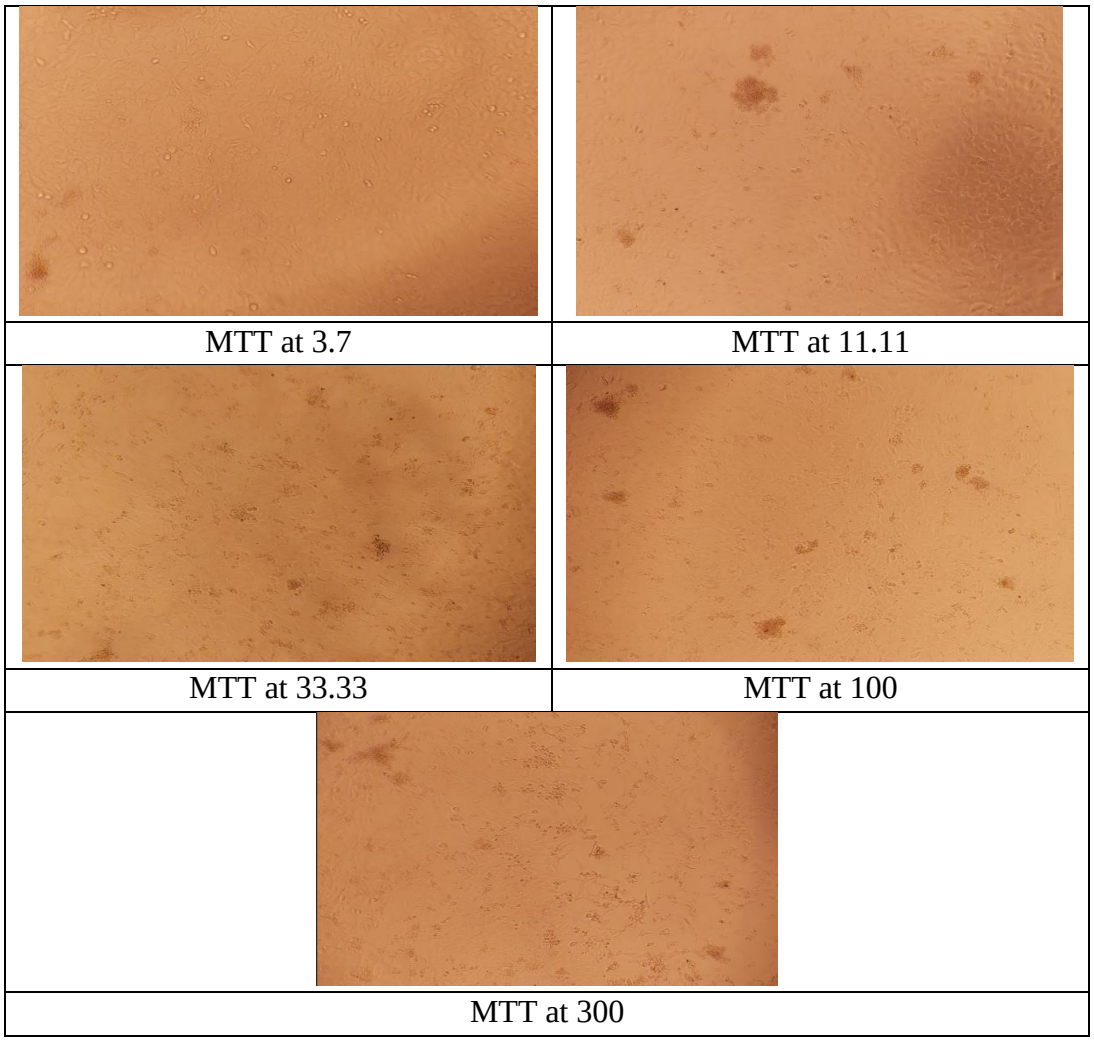

Figure 22. PC-3 cells treated with varying doses of L_1following the addition of MTT.

IRAQI Academic Scientific Journals

AL ZAHRAA UNIVERSITY JOURNAL
Health and Medical Science

*Al-Zahraa Journal for Health and Medical Sciences 2026; 4(1):*14-50 **Vol. 4, No.1, 2026**
www.zjhms.alzahraa.edu.iq

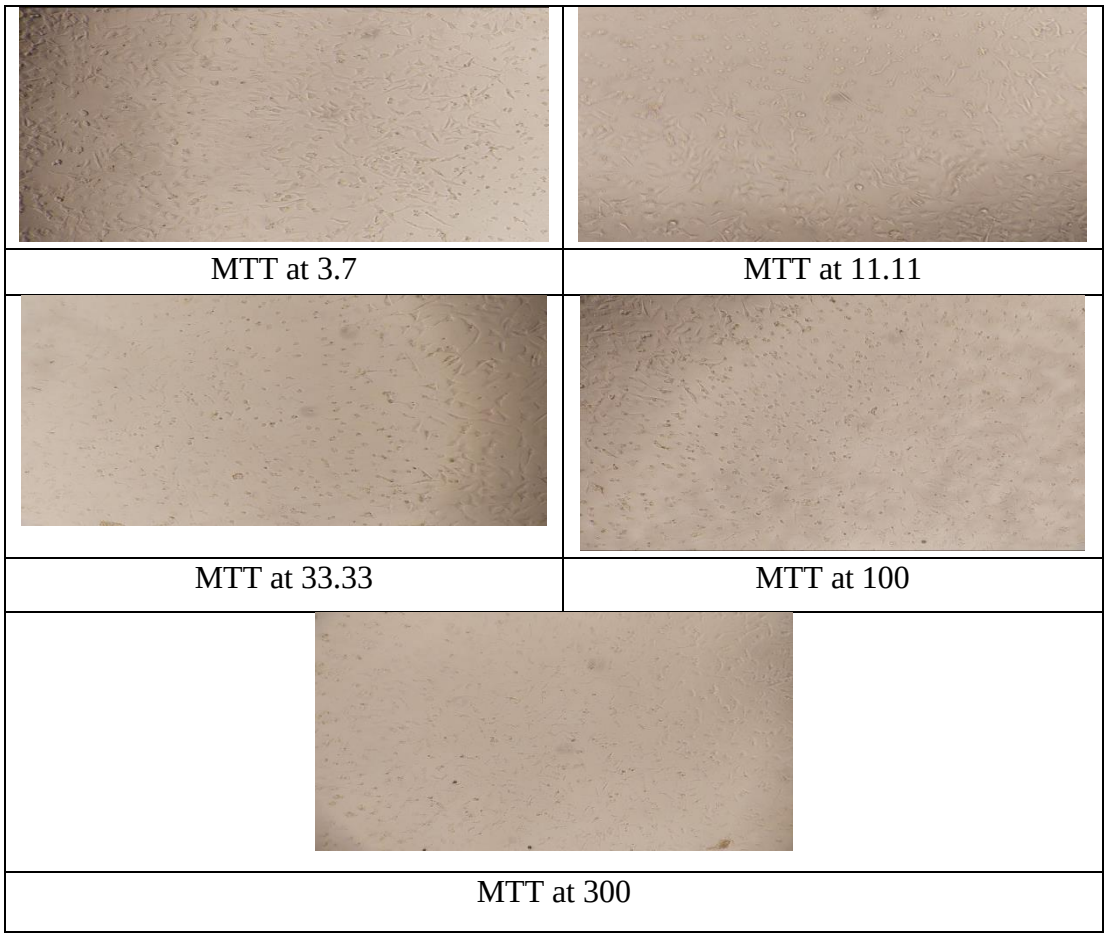

Figure 23. HDF cells treated with varying doses of L_1 following the addition of MTT.

Table 12. MTT test for 24 hours to demonstrate how the gold (III) complex affects the proliferation of prostate cancer cell lines (PC-3) and compares it to the normal cell line (HDF) for the same concentration.

Con. (µg/mL)	Mean Percentage (%) for each cell line					
	PC-3			HDF		
	Cancerous line cells of PC-3			Normal line cells of HDF		
	Cell Viability%	SD	Cell Inhibition %	Cell Viability%	SD	Cell Inhibition %
3.7	89.20	1.17	10.80	93.60	6.74	6.40
11.11	65.12	0.23	34.88	83.84	2.80	16.16
33.33	51.16	0.23	48.84	78.14	4.28	21.86
100	41.20	4.46	58.80	68.02	7.07	31.98
300	35.80	3.64	64.20	56.74	10.85	43.26
IC_{50}= 51.48 µg/mL				**IC_{50}=817.24 µg/mL**		

AL ZAHRAA UNIVERSITY JOURNAL
Health and Medical Science

*Al-Zahraa Journal for Health and Medical Sciences 2026; 4(1):*14-50 **Vol. 4, No.1, 2026**
www.zjhms.alzahraa.edu.iq

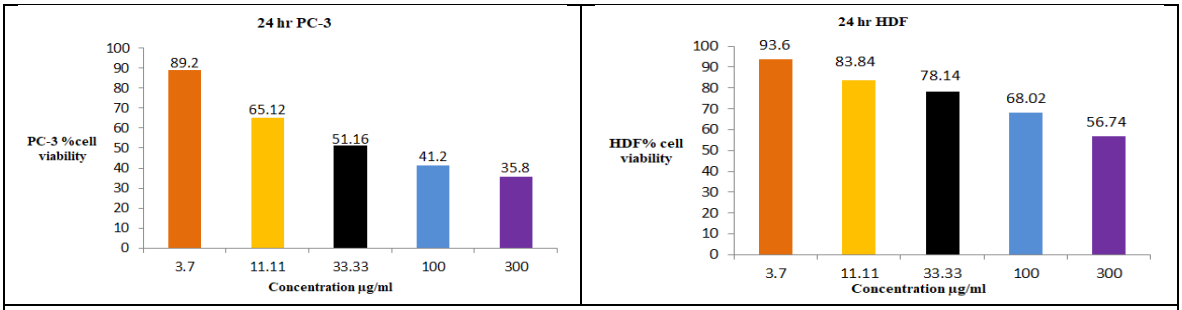

Figure 24. The percentage of living cells (% Cell Viability) for both normal cell line cells (HDF) and prostate cancer cell lines (PC-3) in relation to the complex [Au (L_1)]Cl_3.H_2O concentration.

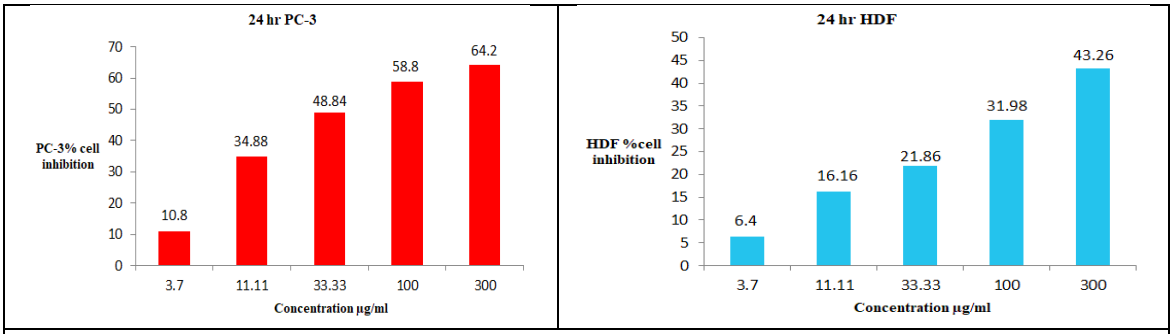

Figure 25.The compound [Au(L_1)]Cl_3.H_2O percentage of inhibition (% Inhibition) on prostate cancer cell lines (PC-3) and normal cell lines (HDF) at varying doses.

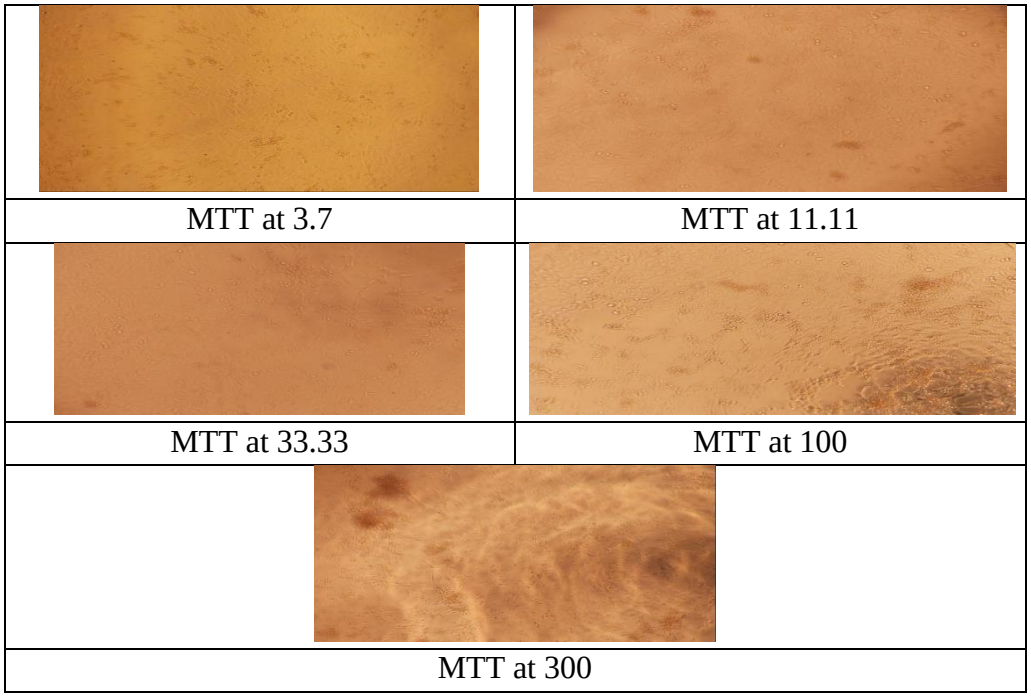

Figure 26. PC-3 cells treated with several doses of [Au(L_1)]Cl_3.H_2O following the addition of MTT.

IRAQI Academic Scientific Journals

AL ZAHRAA UNIVERSITY JOURNAL
Health and Medical Science

*Al-Zahraa Journal for Health and Medical Sciences 2026; 4(1):*14-50 **Vol. 4, No.1, 2026**
www.zjhms.alzahraa.edu.iq

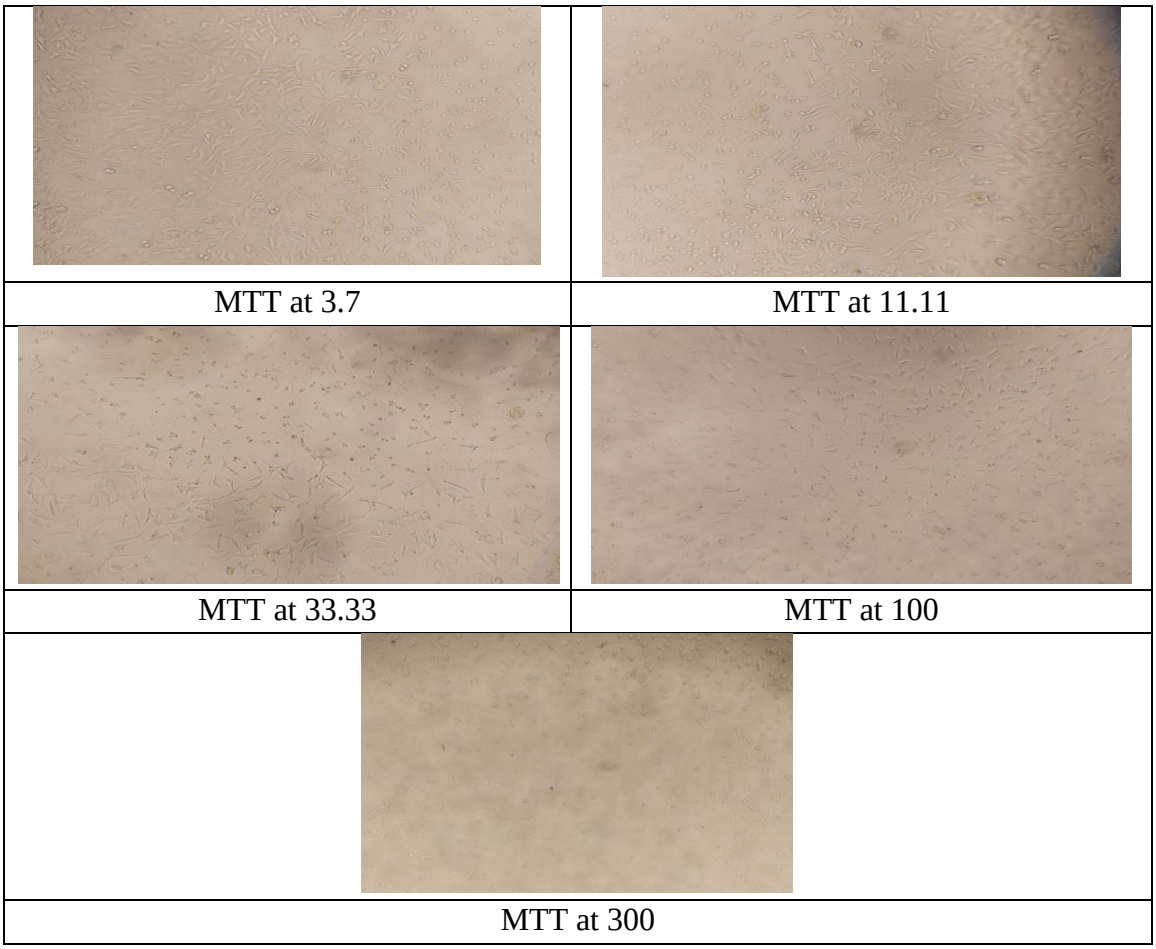

Figure 27. HDF cells treated with varying doses of $[Au(L_1)]C_{l3}.H_2O$ following the addition of MTT.

4. Conclusion

The Nano complexes of metal ions with the new ligand were investigated by means of elemental analysis, metal composition analysis, mass spectrometry, ^{1}HNMR, FT-IR, UV-Vis, XRD and FE-SEM analysis. Electrical conductivity measurements and magnetic susceptibility tests indicated that the octahedral configuration was correct for copper(II)complexes except the gold(III) and silver(I) complex were have square planar and tetrahedral configuration respectively. The proportions of M to L in these structures were 1:1, entirely . The bioactivity information for the compounds demonstrated antibacterial properties, in some instances, anti-cancer properties for the prostate.

5. Acknowledgment

I would like to offer my heartfelt appreciation to the whole staff of the Department of Chemistry, Faculty of Science, University of Kufa. I would also want to thank Dr. Fawzi Yahya

AL ZAHRAA UNIVERSITY JOURNAL
Health and Medical Science

*Al-Zahraa Journal for Health and Medical Sciences 2026; 4(1):*14-50 **Vol. 4, No.1, 2026**
www.zjhms.alzahraa.edu.iq

Wedday for his help throughout this study.

References

1. El-Shalakany, H.H., Ramadan, R.M. and Sayed, M.A. (2023). New bivalent metal chelates based on an NO-donor Schiff base ligand: synthesis, structural characterization, DFT simulation, biological evaluation, and molecular docking analysis. *Inorganic Chemistry Communications*, 159, pp.111826–111826. doi:https://doi.org/10.1016/ j.inoche.2023 .111826.
2. Tavakoli, F. and Zendehdel, M. (2023). Increasing the Acidity of MCM-41 by Functionalized Thiosemicarbazones Schiff- Base Complexes as an Efficient Catalyst for Biginelli Reaction. Silicon. doi:https://doi.org/10.1007/s12633-023-02295-9.
3. Nemec, I., Svoboda, I. and Herchel, R. (2019). Spin Crossover in Three Mononuclear Iron (III) Schiff Base Complexes. Metals, 9(8), p.849. doi:https://doi.org/10.3390/met9080849.
4. Siegel, R.L., Miller, K.D. and Jemal, A. (2019). Cancer statistics, 2019. CA: a Cancer Journal for Clinicians, [online] 69(1), pp.7–34. doi:https://doi.org/10.3322/caac.21551.
5. Smyth, D. (2018). Chronic diseases can increase the risk of developing cancer. Cancer Nursing Practice, 17(2), pp.12–12. doi:https://doi.org/10.7748/cnp.17.2.12.s11.
6. Arriaga-Izabal, D., Morales-Lazcano, F. and Canizalez-Román, A. (2025). Human papillomavirus and prostate cancer in Mexican men: a systematic review and meta-analysis. Cancer Causes & Control, 36(8), pp.755–764. doi:https://doi.org/10.1007/s10552-025-01989-2.
7. El-Gammal, O.A., Mohamed, F.Sh., Rezk, G.N. and El-Bindary, A.A. (2021). Structural characterization and biological activity of a new metal complexes based of Schiff base. Journal of Molecular Liquids, 330, p.115522. doi:https://doi.org/10.1016/j. molliq. 2021.115522.
8. Xing, Y., Li, W., Wang, Q., Li, X., Xu, Q., Guo, X., Bi, X., Liu, X., Shui, Y., Lin, H. and Yang, H. (2019). Antimicrobial Nanoparticles Incorporated in Edible Coatings and Films for the Preservation of Fruits and Vegetables. Molecules, [online] 24(9), p.1695. doi:https://doi.org/10.3390/molecules24091695.

AL ZAHRAA UNIVERSITY JOURNAL
Health and Medical Science

*Al-Zahraa Journal for Health and Medical Sciences 2026; 4(1):*14-50 **Vol. 4, No.1, 2026**
www.zjhms.alzahraa.edu.iq

9. Alfatlawi, I.O., Alrammahi, F.A. and Kelaby, K.K.A.A. - (2022). Synthesis and Identification of New Heterocyclic Compounds from Isatin by Schiff Base Reaction. Global Academic Journal of Pharmacy and Drug Research, 4(1), pp.24–35. doi:https://doi.org/10.36348/ gajpdr. 2022 .v04i01.004.
10. G Siddarth H, S. (2023). Synthesis and Characterization of Some Metal Complexes Prepared from Schiff Base Ligand having Heterocyclic Unit. International Journal of Science and Research (IJSR), 12(8), pp.1871–1874. doi:https://doi.org/10.21275 /sr23818122552.
11. Yogesh Deswal, Sonika Asija, Tufail, A., Dubey, A., Laxmi Deswal, Kumar, N., Jagat Singh Kirar, Neeraj Mohan Gupta and Pinki Barwa (2023). Metal Complexes of 1,2,4-Triazole Based Ligand: Synthesis, Structural Elucidation, DFT Calculations, Alpha-Amylase and Alpha-Glucosidase Inhibitory Activity Along with Molecular Docking Studies. Journal of inorganic and organometallic polymers and materials, 34(1), pp.144–160. doi:https://doi.org/10.1007/s10904-023-02808-4.
12. Jamel, H.O. and Al-Obaidi, N. jawad (2018). Synthesis and Characterization of New Ligand Derived from Benzimidazole and It's Complexes with Some Transition Metals. International Journal of Research in Pharmaceutical Sciences, 9(SPL1). doi:https://doi.org /10.26452/ijrps.v9ispl1.1380.
13. Nasiri Sovari, S. and Zobi, F. (2020). Recent Studies on the Antimicrobial Activity of Transition Metal Complexes of Groups 6–12. Chemistry, 2(2), pp.418–452. doi:https:// doi.org/10.3390/chemistry2020026.
14. KOC, Z.E. (2025). The Synthesis of Hetrocyclic Schiff Bases and Investigation of [(Fe(Salen)Cl] Metal Complexes. The Eurasia Proceedings of Science Technology Engineering and Mathematics, 35, pp.178–183. doi:https://doi.org/10.55549/ epstem.1804538.
15. Ninna Arifatun Nurul Azizah, Hening, M., Sentot Budi Rahardjo and Soerya Dewi Marliyana (2025). Synthesis and Antibacterial Testing of Cu(II)-3-Picolylamine Complexes. Jurnal Kimia Sains dan Aplikasi, [online] 28(5), pp.267–273. doi:https://doi.org/10.14710 /jksa.28.5.267-273.

AL ZAHRAA UNIVERSITY JOURNAL
Health and Medical Science

*Al-Zahraa Journal for Health and Medical Sciences 2026; 4(1):*14-50 **Vol. 4, No.1, 2026**
www.zjhms.alzahraa.edu.iq

16. Pasieczna-Patkowska, S., Cichy, M. and Flieger, J. (2025). Application of Fourier Transform Infrared (FTIR) Spectroscopy in Characterization of Green Synthesized Nanoparticles. Molecules, [online] 30(3), p.684. doi:https://doi.org/10.3390/ molecules 30030684.
17. Sharada, T., Manjunatha, K., Yogeesha, H.C., Harisha, P., Channa Keshava, N.N., Ambika, A.V., Algburi, S., Majdi, A. and Abdulhadi, A.M., 2025. Synthesis, Characterizations of New Schiff Base Heterocyclic Derivatives and their Density Functional Theory (DFT) and Nonlinear Optical (NLO) Studies. *Journal of The Institution of Engineers (India): Series D*, pp.1-11. doi:https://doi.org/10.1007/s40033-025-00969-9.
18. Gemechu Lemecha, Taye, A. and Getachew, N. (2024). Synthesis and structural studies on zinc(II) macrocyclic and hetrocyclic complexes derived from schiff base and mixed ligands of 1,4-dihydroquinoxaline-2,3-dione, orthophenylene diamine and hydroquinone. Bulletin of the Chemical Society of Ethiopia, 39(1), pp.49–64. doi:https://doi.org/10.4314/bcse.v39i1.4.
19. Mahmoud, S.A., Atia, B.M., Amin, L.G. and Abdalla, M. (2024). Innovative preparation of multi-dentate Schiff base adsorbent for the adsorption of silver and its application on nano silver particles preparation from liquid photographic wastes. Journal of Chemical Technology & Biotechnology, 100(2), pp.448–465. doi:https://doi.org/10.1002/jctb.7787.
20. Ayoub, M.A., Fahim, A.M. and Magar, H.S. (2025). Novel Schiff base Cu(ii) and Au(iii) complexes: spectroscopic, computational, and electrochemical insights for H_2O_2 sensor applications. RSC Advances, [online] 15(49), pp.41447–41470. doi:https://doi.org/10.1039/ d5ra06669g.
21. Mahgoub, S. (2018). Synthesis, Characterization and Antimicrobial Activity of Some Novel Quinoline Derivatives Bearing Pyrazole and Pyridine Moieties. Egyptian Journal of Chemistry, 0(0). doi:https://doi.org/10.21608/ejchem.2018.3941.1345.
22. Gomha, S.M., Al-Hussain, S.A., Riyadh, S.M., Farag, B., Abolibda, T.Z., Alrehaili, M.M., Alakhdhari, H.M. and Zaki, M.E.A. (2026). Novel bis-Thiazolidinone -based chalcones with pyridine linker: Eco-friendly synthesis, cholinesterase and beta-amyloid

IRAQI Academic Scientific Journals

AL ZAHRAA UNIVERSITY JOURNAL
Health and Medical Science

*Al-Zahraa Journal for Health and Medical Sciences 2026; 4(1):*14-50 **Vol. 4, No.1, 2026**
www.zjhms.alzahraa.edu.iq

inhibition potency, and molecular docking studies. Bioorganic Chemistry, 168, p.109372. doi:https://doi.org/ 10.1016/j.bioorg.2025.109372.

23. Smirnov, V.G., Lyrshchikov, S.Yu., Manakov, A.Yu., Rodionova, T.V. and Ismagilov, Z.R. (2024). High-resolution 1 H MAS NMR spectra of water sorbed by various types of coals. International Journal of Coal Preparation and Utilization, pp.1–22. doi:https://doi.org /10.1080/19392699.2024.2441841.
24. Mahadik, V.M., Mhaldar, P.M., Patil, M.V., Nerlekar, N.A., Dandge, P.B. and Pore, D.M. (2025). Multicomponent Synthesis of Thiazolidinone -Bis Schiff Base Hybrids and Evaluation of Their Antibacterial and Antioxidant Activity. ChemistrySelect, 10(17). doi:https://doi.org/10.1002/slct.202405332.
25. Yousefshahi, M.R., Abdollah Neshat, Reza Taghizadeh-Tabarsi, Shiva Akbari-Birgani and Fahimeh Varmaghani (2025). A novel ligand system comprising N-heterocyclic carbene and Schiff base ligands: spectroscopic and electrochemical analysis, investigation of silver and gold complexation, and their biological effects. New Journal of Chemistry, [online] 49(5), pp.1736–1744. doi:https://doi.org/10.1039/d4nj04482g.
26. Fatimah, S., Ragadhita, R., Husaeni, D.F.A. and Nandiyanto, A.B.D. (2021). How to Calculate Crystallite Size from X-Ray Diffraction (XRD) using Scherrer Method. ASEAN Journal of Science and Engineering, 2(1), pp.65–76. doi:https://doi.org/10.17509/ ajse .v2i1.37647.
27. Synthesis, Characterization And Antibacterial Analysis Of Benzocaine Schiff Base Metal Complexes. (2024). Nanotechnology Perceptions, 20(6). doi:https://doi.org/10.62441/nano-ntp.v20i6.70.
28. Ali, A.B.M., Abdulsalam Abdulsattar Abdulazez, Elyor Berdimurodov, Singh, N., Rusho, M.A., Aseel Smerat, Diab, M.A., El-Sabban, H.A., Arabi, A. and Islam, S. (2025). Bio-supported of gold nanoparticles over magnetic nanoparticles: Synthesis, characterization and evaluation its catalytic activity for one-pot preparation of pyrano[2,3-d]pyrimidines. Journal of Organometallic Chemistry, 1038, pp.123759–123759. doi:https://doi.org/10.1016/j. jorganchem.2025.123759
29. Almehizia, A.A., Naglah, A.M., Aljafen, S.S., Hassan, A.S. and Aboulthana, W.M. (2025). Assessment of the In Vitro Biological Activities of Schiff Base-Synthesized

AL ZAHRAA UNIVERSITY JOURNAL
Health and Medical Science

*Al-Zahraa Journal for Health and Medical Sciences 2026; 4(1):*14-50 **Vol. 4, No.1, 2026**
www.zjhms.alzahraa.edu.iq

Copper Oxide Nanoparticles as an Anti-Diabetic, Anti-Alzheimer, and Anti-Cancer Agent. Pharmaceutics, [online] 17(2), pp.180–180. doi:https://doi.org/10.3390/pharmaceutics17020180.

30. Caviglia, M., Li, Z., Santini, C., Del Gobbo, J., Cimarelli, C., Du, M., Dolmella, A. and Pellei, M. (2025). New Cu(II), Cu(I) and Ag(I) Complexes of Phenoxy-Ketimine Schiff Base Ligands: Synthesis, Structures and Antibacterial Activity. Molecules (Basel, Switzerland), [online] 30(9), p.1893. doi:https://doi.org/10.3390/molecules30091893.
31. Ramakrishna Reddy, K. and Gosu, N.R. (2025). Review on synthesis protocols, anti-bacterial and photovoltaic applications of novel Schiff-base metal complexes. Results in Chemistry, 16, p.102404. doi:https://doi.org/10.1016/j.rechem.2025.102404.
32. Mohamed Nasar, N., Samuel, M., Selvaraj, F.S.S., Alagumuthu, M., Jeyaraman, P. and Raman, N. (2025). Remarkable drug-like properties of mixed ligand coordination compounds having dicarboxylic acid: synthesis, characterization, molecular docking and DFT studies. Nucleosides, Nucleotides & Nucleic Acids, pp.1–27. doi:https://doi.org/10.1080/15257770.2025.2552942.
33. Gaber, A., Alsanie, W.F., Kumar, D.N., Refat, M.S. and Saied, E.M. (2020). Novel Papaverine Metal Complexes with Potential Anticancer Activities. Molecules, 25(22), p.5447. doi:https://doi.org/10.3390/molecules25225.